A ground-to-exosphere Martian general circulation model: 2. Atmosphere during solstice conditions—Thermospheric polar warming

F. González-Galindo,[1] F. Forget,[1] M. A. López-Valverde,[2] and M. Angelats i Coll[1]

Received 8 October 2008; revised 16 April 2009; accepted 8 May 2009; published 25 August 2009.

[1] A ground-to-exosphere Martian general circulation model is applied to study the thermal and dynamical structure of the upper Martian atmosphere during solstitial conditions. Special attention is paid to the reproduction of the thermospheric polar warming observed by Mars Odyssey during southern hemisphere (SH) summer solstice. The intensity and latitudinal distribution of this polar warming are successfully reproduced by the model. The heating balance and the dynamical structure of the upper atmosphere are studied. It is shown that a strong interhemispheric transport produces a convergence and descent of air over the winter pole, producing an adiabatic heating and a polar warming. This structure confirms previous results made by other models. The most novel aspect of this study is a sensitivity study showing the importance of the tides excited in situ in the upper atmosphere. These tides are critical to the simulated thermal and dynamical structure and remain key components of the interhemispheric transport mechanism responsible for the thermospheric polar warming. The day-night temperature differences created by these in situ tides produce a day-night transport that reinforces the summer-to-winter circulation and the descent of air over the pole, becoming an essential factor for this thermospheric polar warming. The effect of upward propagating nonmigrating tides is also studied.

Citation: González-Galindo, F., F. Forget, M. A. López-Valverde, and M. Angelats i Coll (2009), A ground-to-exosphere Martian general circulation model: 2. Atmosphere during solstice conditions—Thermospheric polar warming, *J. Geophys. Res.*, *114*, E08004, doi:10.1029/2008JE003277.

1. Introduction

[2] In a previous paper [*González-Galindo et al.*, 2009], hereafter referred to as paper 1, we described in detail the extension to the thermosphere of the general circulation model (GCM) of the Martian atmosphere developed at the Laboratoire de Météorologie Dynamique (CNRS, Paris). A study of the seasonal, solar cycle, diurnal, and day-to-day variations of the temperatures in the upper atmosphere was presented.

[3] In this paper we apply this model to simulate one of the most significant observations about the Martian upper atmosphere: the thermospheric polar warming (hereafter TPW), first observed during the aerobraking of Mars Odyssey [*Keating et al.*, 2003]. A good review of its characteristics can be found in the work by *Bougher et al.* [2006]. In short, during perihelion conditions, with the periapsis of the orbit above the north polar region, an increase of temperature from 110 K at 60°N to 160–170 K at the pole was observed at 120 km. During the opposite aphelion season, the aerobraking data sets do not show any clear TPW. However, recent observations by SPICAM on Mars Express using the stellar occultation data set suggest a moderate 20–30 K polar warming at this aphelion season between 70 and 115 km [*Forget et al.*, 2009]. Additionally, density measurements at 180 km for about 4 Martian years using electron reflectrometry on MGS show evidence of this aphelion TPW during some years, but not others [*Lillis et al.*, 2008].

[4] On the modeling side, the TPW has been studied using the Mars Thermospheric GCM (MTGCM) coupled to the lower-atmosphere NASA/Ames MGCM [*Bougher et al.*, 2006; *Bell et al.*, 2007] that provides lower-boundary conditions for the thermospheric model. These coupled models predicted a TPW similar to that observed at perihelion, and no warming at aphelion. The TPW was attributed to the adiabatic heating produced by the subsiding branch of a strong interhemispheric circulation cell during the solstices that produces a convergence and downwelling of air over the winter polar region. The seasonal behavior of the TPW was explained by a more efficient interhemispheric transport, and thus a more intense adiabatic warming at the poles, during perihelion, due to stronger insolation and dust heating under these conditions [*Bougher et al.*, 2006]. Further work with these coupled models showed that the interannual variation of the dust load of the atmosphere has

[1] Laboratoire de Météorologie Dynamique, Institute Pierre Simon Laplace, Paris, France.
[2] Instituto de Astrofísica de Andalucía, CSIC, Granada, Spain.

0148-0227/09/2008JE003277

an important effect over the thermal structure of the thermosphere and in particular produced variations in the intensity of the TPW [*Bell et al.*, 2007], showing the importance of the coupling between the lower atmosphere and the upper atmosphere for a correct simulation of this phenomenon. During aphelion, their model showed a weak polar warming at 120 km of 20–30 K, consistent with SPICAM observations.

[5] Although it reproduces satisfactorily the basic features of the TPW, the MTGCM tends to overestimate temperatures in the polar regions, with predicted temperatures being 20–30 K higher than observed [*Bougher et al.*, 2006]. Additionally, these studies did not address questions such as the role of the tides in the generation of the TPW. For these reasons, we think that further study of this phenomenon is useful. The use of a "whole atmosphere" model, as it is the ground-to-exosphere GCM developed at the LMD, removes the need for an artificial boundary between two separate codes [*Bougher et al.*, 2008] and eliminates the problematic differences in radiative parameterizations between coupled models, as a consistent radiative transfer can be used [*Angelats i Coll et al.*, 2005]. So, we believe that the use of a single ground-to-exosphere model is an important improvement that can contribute to a better understanding of the TPW.

[6] Previous observational and theoretical studies have shown the important role of tides in the upper atmosphere structure in Mars [e.g., *Angelats i Coll et al.*, 2004; *Withers et al.*, 2003; *Forbes*, 2004; *Wilson and Hamilton*, 1996; *Forbes et al.*, 2002; *Wilson*, 2000, 2002; *Moudden and Forbes*, 2008a, 2008b]. In particular, it has been shown that the longitudinal variation of the density field sampled by MGS measurements during aerobraking is due to eastward propagating diurnal waves [e.g., *Forbes and Hagan*, 2000; *Wilson*, 2002; *Angelats i Coll et al.*, 2004]. A similar origin is attributed to the longitudinal structure of electron densities measured by MGS occultation [*Bougher et al.*, 2004]. All of these works also show that the nonmigrating components (as, e.g., the diurnal Kelvin wave), excited mainly by the interaction of the diurnal tide with the topography (in Mars the large topographic relief is dominated by a zonal wave number 2 component), have a significant contribution to the tidal structure of the upper atmosphere [*Forbes and Hagan*, 2000; *Angelats i Coll et al.*, 2004; *Moudden and Forbes*, 2008b]. Their long vertical wavelengths allow them to propagate up to high altitudes (i.e., the thermosphere) before they dissipate, affecting the temperature and wind field in the upper atmosphere [e.g., *Wilson*, 2000; *Moudden and Forbes*, 2008a, 2008b]. An excellent review of the role of the tides in terrestrial planetary atmospheres can be found in the work of *Forbes* [2002].

[7] Our aim here is the study of the TPW, and in particular the influence of the tides, especially those created in situ in the upper atmosphere by the absorption of solar NIR and UV radiation, on the thermal and dynamical structure of the upper atmosphere, and their role in the creation of the TPW.

[8] In section 2 we analyze the thermal and dynamical state, as well as the thermal balance, of the Martian upper atmosphere during solstitial conditions, paying special attention to the TPW. Some numerical tests were performed to allow for a deeper understanding of the processes that produce the TPW. In particular, we present the results of a simulation suppressing the excitation of in situ generated upper atmospheric tides, and its implications for the TPW, in section 3.1. Another experiment where the creation of nonmigrating tides in the lower atmosphere is inhibited is presented in section 3.2. Finally, the conclusions of this study are summarized in section 4.

2. Simulated Thermospheric Polar Warming

[9] For this study, we use the results for the L_s = 270–300 "month" of the 1-year simulation already described in paper 1. This temporal interval corresponds approximately to the orbital conditions of Mars Odyssey aerobraking. We will use the time-averaged results created using the procedure described in paper 1, so that a "typical day" is obtained. As in paper 1, we will study the results for Universal Time UT = 12 (i.e., midday at geographic longitude 0), which eases the interpretation of the results. No significant differences are obtained if another UT is chosen.

[10] The zonal mean temperature predicted by the LMD-MGCM for this period as a function of pressure and latitude, already shown in Figure 3 of paper 1, can be seen in Figure 1. The basic features of the vertical structure of the atmosphere, such as the minimum of temperature of the mesopause, and the increase of temperature with altitude characteristic of the lower thermosphere, already commented in paper 1, are easily identified. Maximum temperatures in the thermosphere of about 320 K are obtained in the summer midlatitudes and high latitudes, corresponding, as we will see in section 2.1, to the area of maximum radiative (UV + NIR) heating. Focusing on the mesopause/lower-thermosphere level, between 10^{-2} Pa and 10^{-4} Pa, a prominent feature, and a major topic of this work, is the increase of temperature when going from midlatitudes to the pole in the winter (northern) hemisphere. At the mesopause altitude, the temperature increases from about 125 K at 30°N to more than 160 K at the pole. The polar warming in the lower atmosphere is also clearly visible. An intense warming in the lower atmosphere, associated with a major dust event, was observed by the Viking Infrared Thermal Mapper (IRTM) [*Jakoski and Martin*, 1987] (that sensed a depth-weighted temperature centered at roughly 0.5 hPa, or about 25 km) and simulated by *Wilson* [1997] and *Forget et al.* [1999] (with a version of the LMD-MGCM extended up to 90 km only). It is originated by a quasi-global Hadley cell, characterized by strong poleward meridional winds that induce a mass convergence and an adiabatic warming over the winter pole [*Forget et al.*, 1999]. TES observations [e.g., *Smith et al.*, 2001] show a more modest warming above about 3 Pa, similar to the one predicted by the model.

[11] In order to make the comparison with the TPW measured by Mars Odyssey it is convenient to use altitude as the vertical coordinate, instead of pressure levels. However, we will need to keep in mind when using constant altitude levels the effect of the atmospheric inflation/contraction. This effect can be especially important in the winter polar regions: the very low temperatures of the lower atmospheric layers can produce a strong contraction of the whole atmosphere, so that a constant altitude layer that in midlatitudes corresponds to the mesopause may correspond

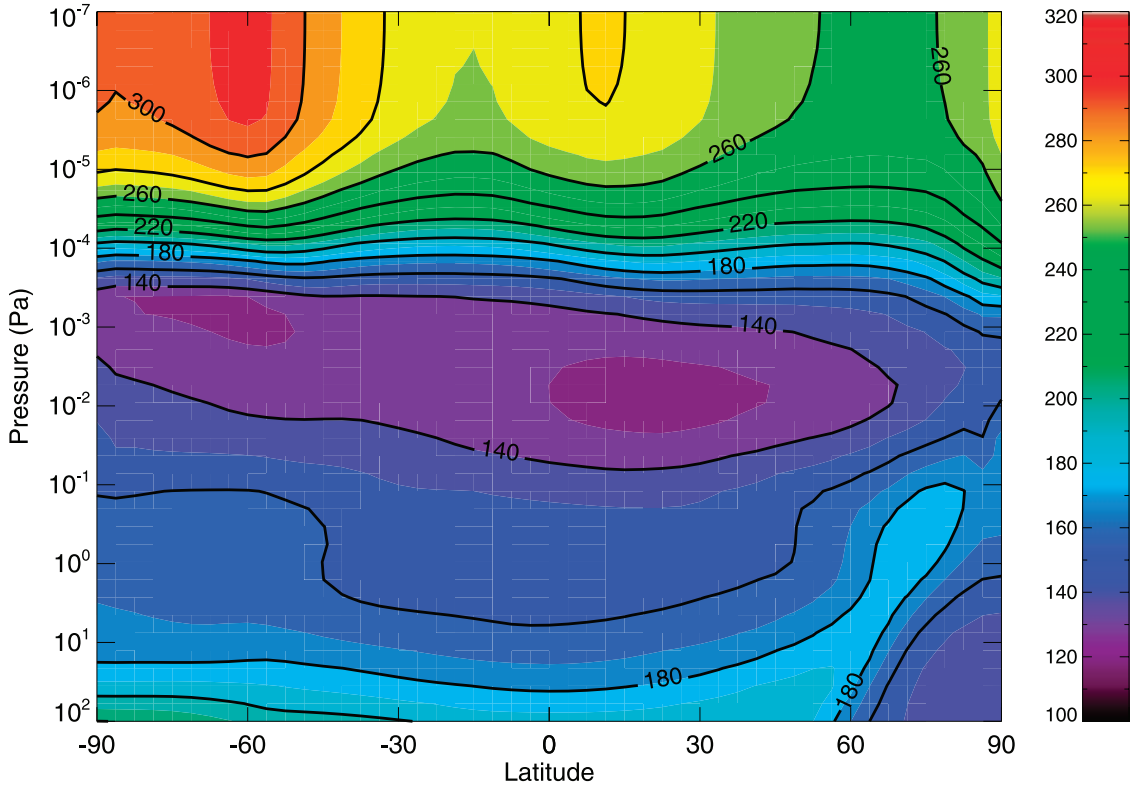

Figure 1. Latitude-pressure cross section of the zonally averaged temperature for L_s = 270–300.

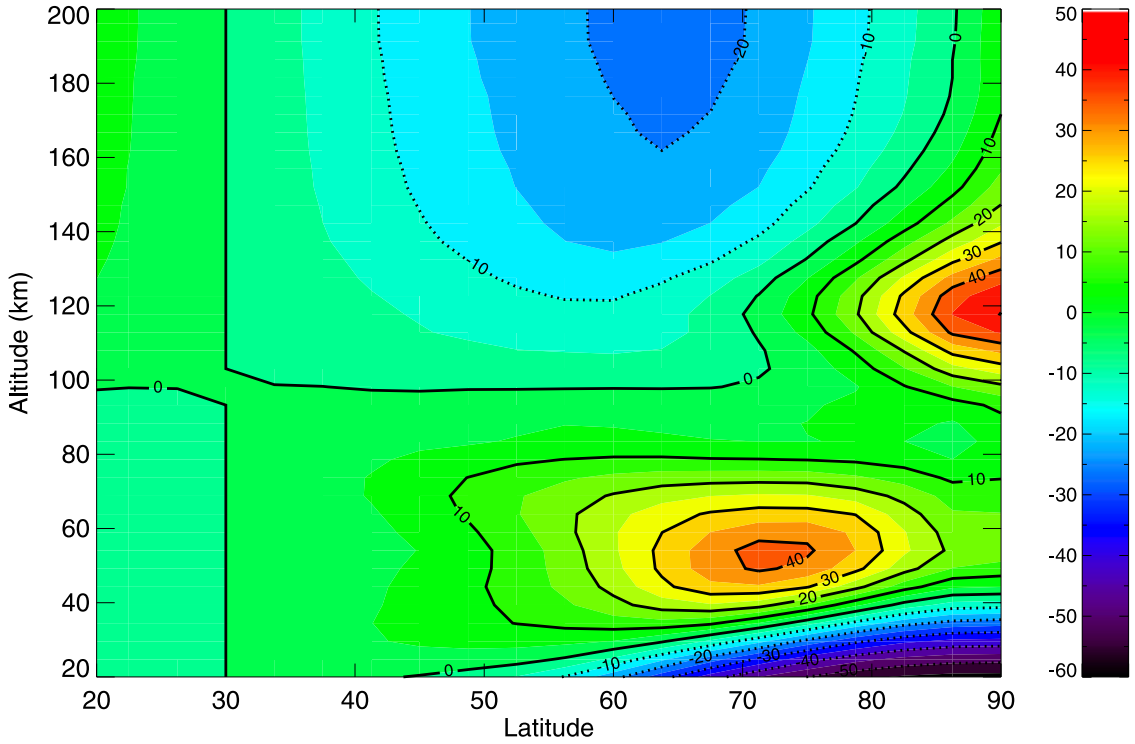

Figure 2. Cross section of the increase of zonal mean temperature at each latitude from reference at latitude = 30°N, as a function of altitude, for L_s = 270–300.

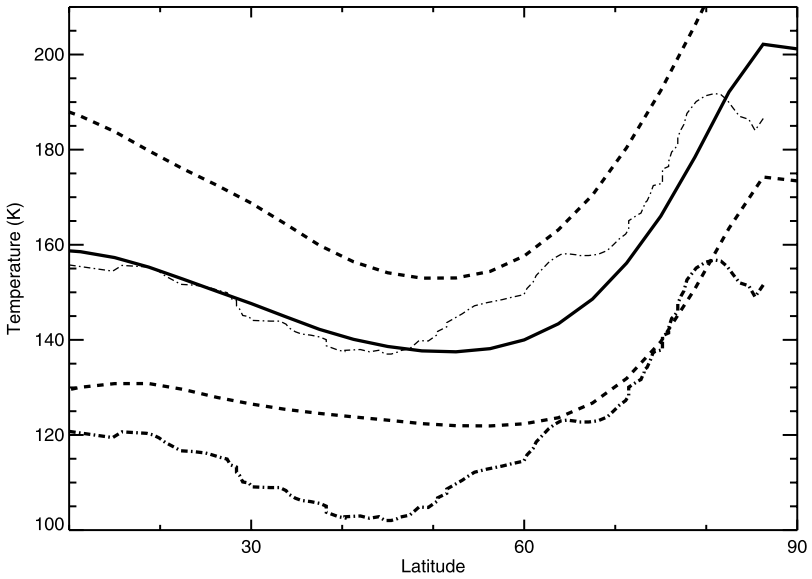

Figure 3. Zonal mean temperature predicted by the model at constant local time = 2 and 120 km of altitude for the L_s = 270–300 seasons (solid line) plus or minus its standard deviation (dashed lines). Nightside temperature (thick dash-dotted line) observed by Mars Odyssey at 120 km, from *Bougher et al.* [2006]. Thin dash-dotted line is same as thick dash-dotted line, but offset by 35 K.

to the lower thermosphere in polar regions. Given the sharp increase of temperature at these altitudes, the temperature at this constant altitude layer at the pole can be significantly higher than in midlatitudes, even without the intervention of an adiabatic warming. This effect contributes to the observed TPW, as discussed in section 3.1.

[12] The magnitude and distribution of the polar warming can be better appreciated in Figure 2, where we depict the increase of temperature from latitude = 30°N to the winter pole as a function of altitude and latitude. Two different areas of warming can be clearly distinguished: one in the lower atmosphere, at about 50 km of altitude, and another one in the upper atmosphere with a maximum at 120 km of altitude. Both have a similar magnitude, more than 40 K, but their latitudinal distribution is different: while the warming in the lower atmosphere is centered at latitude 70°N, and decreases when getting closer to the pole, the one in the upper atmosphere has a maximum in the polar region. The former is the lower-atmosphere polar warming, already mentioned in paper 1 and described by *Forget et al.* [1999]. The latter is the TPW observed by Mars Odyssey, on which we will focus.

[13] In order to compare the TPW predicted by our model with the one observed by Mars Odyssey it is necessary to reproduce as closely as possible the conditions of the observations. In particular, most of the MO observations were made at nightside, with local time (LT) close to 0200. The polar warming predicted by our model at constant LT = 2 and at constant altitude of 120 km during the L_s = 270–300 season is shown in Figure 3 (black line), together with the observations of MO (thick dash-dotted line), taken from Figure 1 of *Bougher et al.* [2006]. The polar warming predicted by our model is of about 60 K at 120 km, with temperature increasing from about 140 K at latitude ≈ 55°N to more than 200 K close to the pole. Both the magnitude and latitudinal structure of the predicted polar warming is in good agreement with the observations, which show an increase of temperature from about 105 K at 45°N to 160 K at 80°N [*Bougher et al.*, 2006]. However, predicted temperatures are 30 to 40 K higher than observed, as can be seen when comparing the prediction of the model (black line) with the temperature observed by MO offset by 35 K (thin dash-dotted line). MTGCM simulations showed a similar overestimation of the temperature by about 30 K [*Bougher et al.*, 2006], as commented in section 1. An overestimation of the temperatures predicted by the LMD-MGCM at the mesopause/lower thermosphere, of similar magnitude, was also found during the comparison with SPICAM temperature profiles [*Forget et al.*, 2009], as stated in paper 1. This is attributed to an underestimation of the 15 μm cooling due to the effect of collisions with atomic oxygen. We refer the reader to those papers for a deeper discussion on the possible origin of this overestimation.

[14] For the northern summer (NH) season, the latitudinal variation of the temperature at LT = 2 and constant altitude of 100 km is shown in Figure 4. The warming is now smaller than in the southern summer season, with temperatures increasing from about 125 K at 30°N to less than 160 in the winter pole. Although MGS observed no signal of a TPW during this season, with measured temperatures as low as 90 K, other more recent measurements suggest a modest warming during northern summer. In particular, Mars Reconnaissance Orbiter (MRO) detects a small 10 K TPW at 110 km [*Keating et al.*, 2008], and SPICAM-retrieved temperature shows a polar warming of about 20 K in the upper mesosphere. Simulations with the MTGCM also show a warming at aphelion, although less intense, between 14 and 24 K, depending on the dust distribution. Note that again the temperatures obtained with our model at 100 km are higher than the measured ones, and similar to those obtained with the MTGCM at 120 km. Again, this confirms

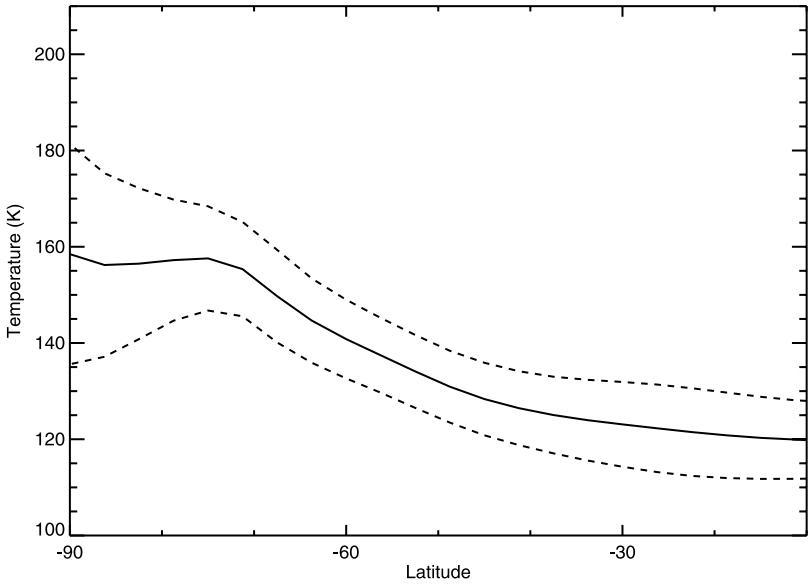

Figure 4. Zonal mean temperature predicted by the model at constant local time = 2 and 100 km of altitude for the L_s = 90–120 seasons (solid line) plus or minus its standard deviation (dashed lines).

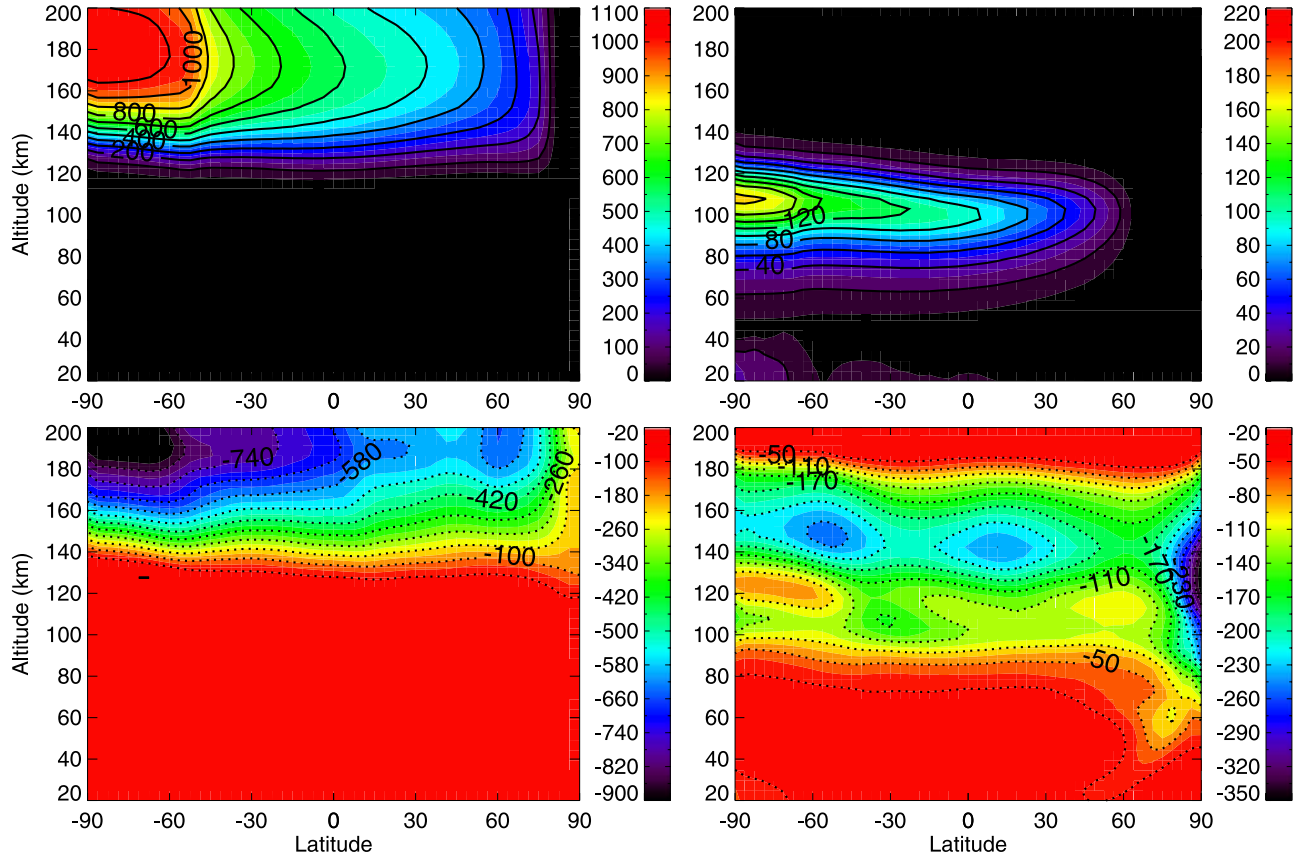

Figure 5. Latitude-altitude cross sections of the zonally averaged (top left) UV heating, (top right) NIR heating, (bottom left) thermal conduction, and (bottom right) 15 μm cooling, in K/d, given by the LMD-MGCM. L_s = 270–300.

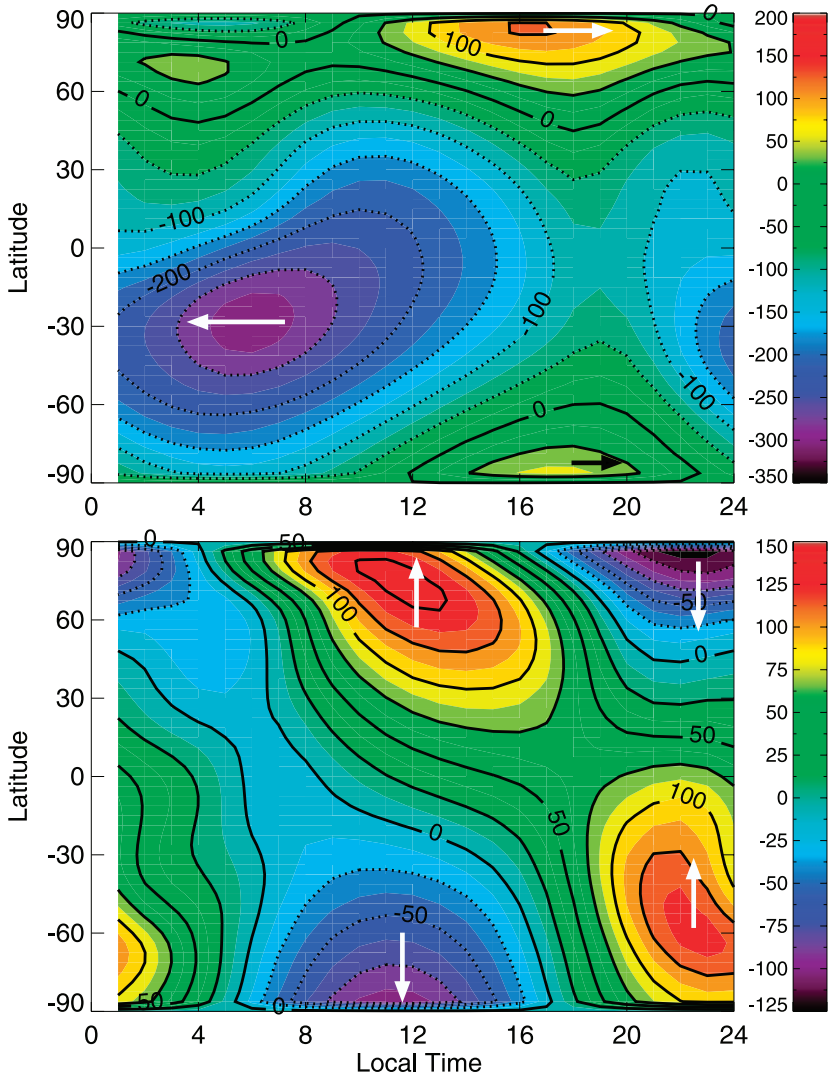

Figure 6. Local time-latitude cross sections of the Sun-synchronous (top) zonal and (bottom) meridional winds (m/s) predicted by the model at 120 km. Arrows have been added to show the wind direction. L_s = 270–300.

that our model overestimates the temperature in the upper mesosphere–lower thermosphere region and underestimates the altitude of the mesopause [*Forget et al.*, 2009]. For the rest of the paper, we will focus on the southern summer season.

2.1. Thermal Balance in the Upper Atmosphere

[15] To analyze the TPW, let us consider the thermal balance of the upper atmosphere. The balance between the radiative heating/cooling terms and the thermal conduction, that previous works have shown to be dominant in the upper atmosphere [*Bougher et al.*, 1999], is shown for our model in Figure 5. Their implementation in the LMD-MGCM is described in paper 1. The UV heating is dominant in the upper layers, above about 130 km, with maximum zonal mean heating of more than 1100 K/d at about 190 km in the summer pole, due to the constant illumination there. It is mainly compensated for by the molecular thermal conduction, which is more efficient in the rarefied upper atmosphere, given its inverse dependence with density (see paper 1). The distribution of the thermal conduction cooling clearly mirrors that of the UV heating. The NIR heating is the dominant heating term between about 70 and 130 km. As for the UV heating, it only occurs during daylight hours, and its latitudinal variation shows a maximum in the constantly illuminated polar summer region. The maximum heating rate is about 200 K/d at about 110 km, much lower than the maximum UV heating. The 15 μm cooling has an important contribution to the heating/cooling balance in the upper mesosphere–lower thermosphere region, between about 80 and 180 km. In fact, it is the dominant cooling term below about 150 km. Although this cooling term has a complex dependence on temperature, the areas of maximum 15 μm cooling are linked to the areas of maximum temperature [*López-Puertas and López-Valverde*, 1995], and therefore it cannot produce a warming. This heating balance is in good agreement with that obtained by the MTGCM [e.g., *Bougher et al.*, 1999].

[16] Focusing again on the winter pole region, it is clear that none of these heating/cooling terms can explain the

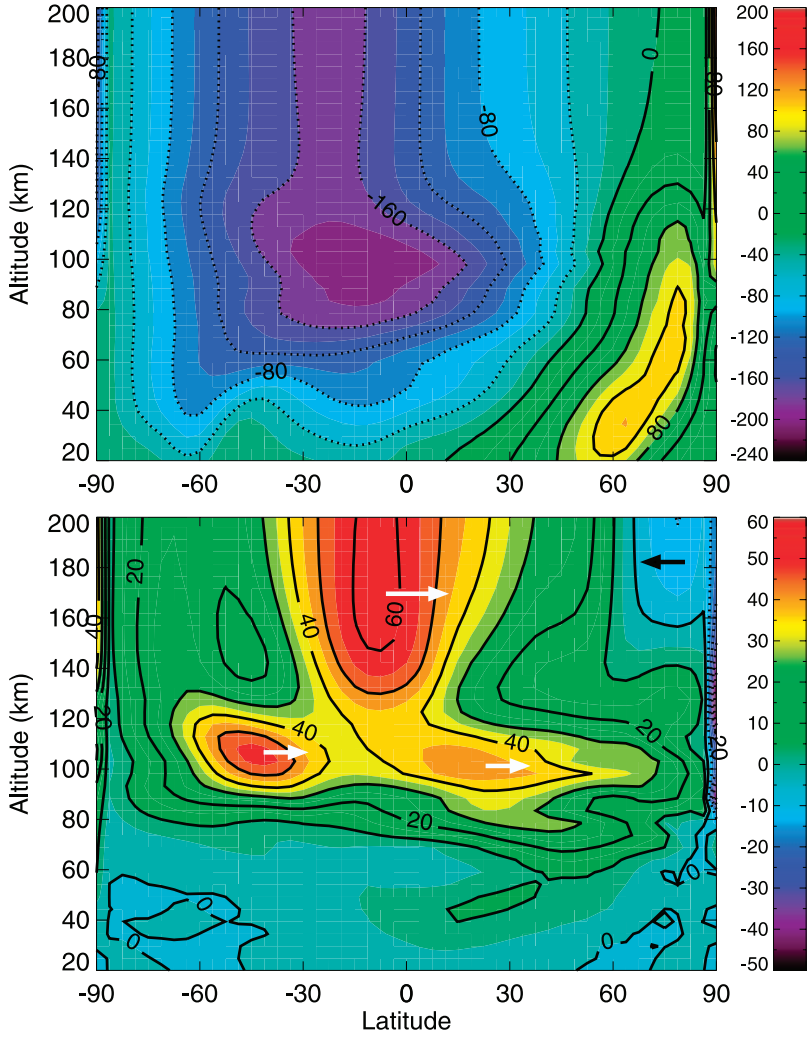

Figure 7. Latitude-altitude cross section of zonally averaged (top) zonal and (bottom) meridional winds (m/s) predicted by the model. Arrows have been added to show the wind direction L_s = 270–300.

high temperatures found in the mesopause/lower thermosphere during the polar night, i.e., the TPW. Neither the UV heating nor the NIR heating act during the polar night, and the 15 μm cooling rate has a maximum at this region, owing to the large temperatures.

2.2. Global Wind Fields

[17] As described in section 1, previous works [*Bougher et al.*, 2006; *Bell et al.*, 2007] showed that the dynamical structure at the upper atmosphere, in particular the enhanced interhemispheric transport during NH winter solstice, is a key factor for the creation of the TPW. The zonally averaged zonal and meridional winds predicted by our model at 120 km during the L_s = 270–300 seasons can be seen in Figure 6 as a function of local time and latitude. It is convenient to remind here that all the results for this season are obtained by compositing a diurnal cycle from the outputs of the model. That is, the results for each day in the season are averaged at given values of the Universal Time (UT) and merged into a single file to obtain a "typical day" for the month. The zonal winds are predominantly westward, except in the polar regions, where there are two eastward jets, more pronounced in the winter pole. Maximum westward wind intensity is more than 350 m/s at low latitudes. The structure of the meridional winds, with northward (southward) winds dominating in the dayside northern (southern) hemisphere and the nightside southern (northern) latitudes, indicates a strong divergence of winds from the midlatitudes of the summer hemisphere in the dayside, with winds passing over the poles and converging in midlatitudes and high latitudes of the winter hemisphere in the nightside. This dynamical pattern is similar to that obtained in the thermosphere with the MTGCM [*Bougher et al.*, 2000]. Maximum wind intensity is about 175 m/s.

[18] This behavior of the meridional winds is indicative of a net transport of matter from the dayside summer hemisphere to the nightside winter hemisphere. This is confirmed by the analysis of the vertical structure of the zonally averaged winds, shown in Figure 7. The zonal averages of the zonal winds are predominantly westward, with an eastward jet in the winter pole at the lower atmosphere, which decreases its intensity when going to upper layers, reversing to weak westward winds above about 140 km. The zonally averaged meridional winds are

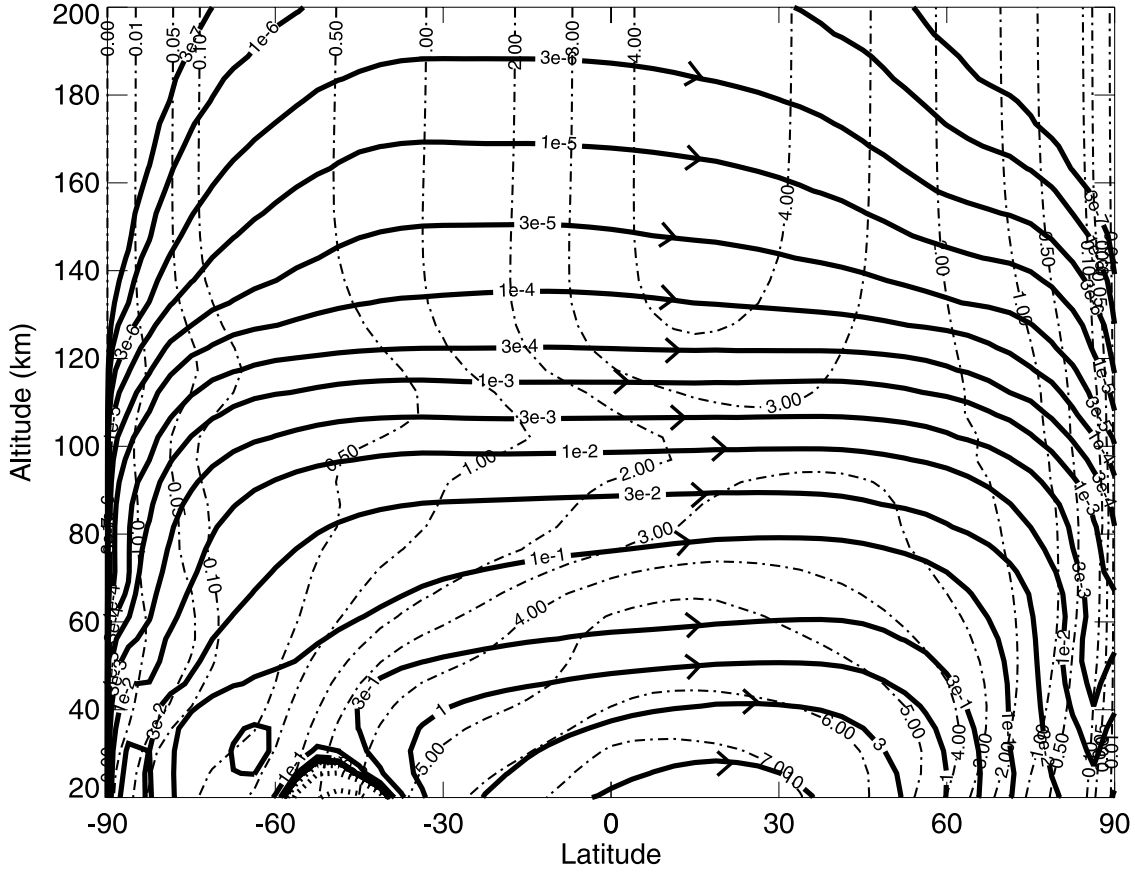

Figure 8. Latitude-altitude contours of mass stream function (thick solid (positive) and dashed (negative) lines, in units of 10^9 kg/s) and angular momentum (thin dash-dotted lines, 10^8 kg m^2/s). L_s = 270–300.

northward almost everywhere, resulting in a net transport from the summer (southern) hemisphere to the winter (northern) one, and confirming the importance of the interhemispheric transport. Meridional winds show a maximum between approximately 90 and 120 km, the altitude of the mesopause, coincident with the altitude where the TPW is predicted (see Figure 2). Another maximum is predicted in the equatorial thermosphere.

[19] The importance of this meridional transport can be better appreciated in Figure 8, where we present the mass stream function (solid thick lines). Clearly, the meridional circulation above about 80 km is characterized by a strong pole-to-pole transport. This is in good agreement with previous results by *Bougher et al.* [2006] and *Bell et al.* [2007].

[20] The zonal mean vertical winds, shown in Figure 9, are positive (upward) in the summer hemisphere and negative (downward) in the winter hemisphere, with maximum descending winds of about 75 cm/s at the mesopause altitude in the winter pole. In the winter polar region there is a significant penetration of air descending from the thermosphere into the mesosphere, with significant vertical velocities down to about 60 km. This result is another proof of the coupling between the upper and the lower atmosphere. Although most of these couplings act from the lower to the upper atmosphere, in this case the direction is the opposite, showing that the thermal and dynamical state of the upper atmosphere can have an effect over the lower atmosphere.

[21] Maybe the most significant effect is that this convergence and descent of air over the winter pole produces, as indicated by *Bougher et al.* [2006], a compressional adiabatic heating. This heating term, as given by our model, can be seen in Figure 10 (top). In the summer hemisphere, the ascending air produces a cooling of the atmosphere, maximum close to the pole. In the winter hemisphere, where the vertical winds are predominantly downward, there is a warming of the thermosphere. This is particularly intense in the polar region, with maximum heating rate of about 600 K/d at about 140 km. A comparison with the sum of the heating terms discussed in section 2.1, presented in Figure 10 (bottom), shows that the adiabatic heating/cooling is able to compensate the effect of the radiative terms plus the thermal conduction. Clearly, this adiabatic heating is at the origin of the TPW, indicating the importance of the penetration of air from the thermosphere into the upper mesosphere, reaching altitudes as low as about 70 km.

[22] To summarize, the structure of the dynamics above about 80 km is as follows: ascending motion in the summer hemisphere, with transport from the summer to the winter hemisphere at thermospheric altitudes, and strong descending motion over the winter pole, down to the mesosphere, producing a strong adiabatic heating in the polar region.

[23] This is in good qualitative agreement with the transport predicted by the MTGCM [*Bougher et al.*, 2006;

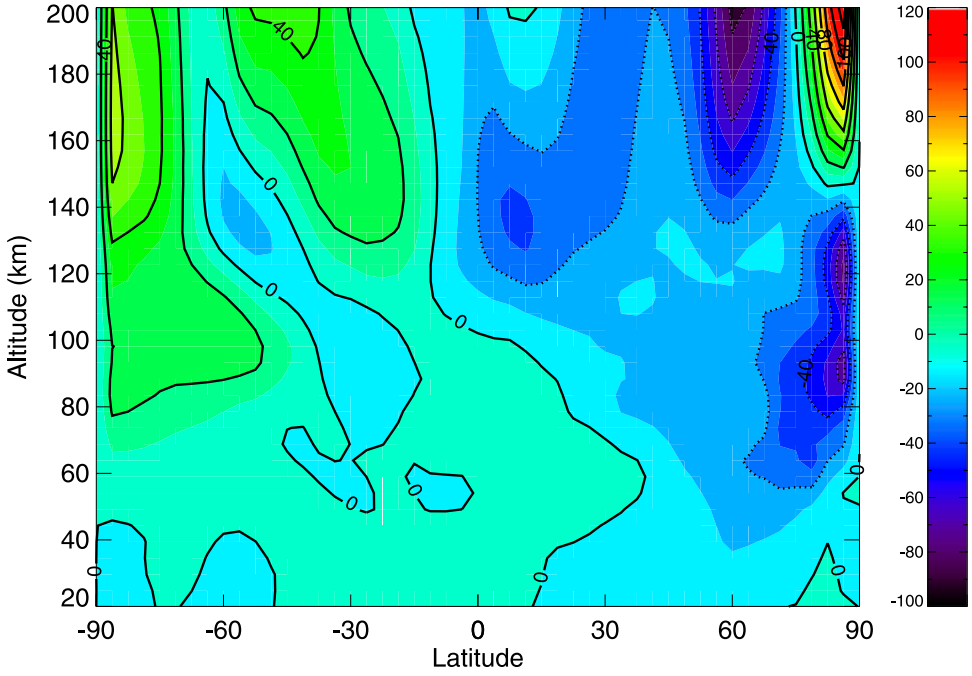

Figure 9. Latitude-altitude cross section of zonally averaged vertical wind (cm/s, positive upward) predicted by the model, L_s = 270–300.

Bell et al., 2007]. However, these authors reported much higher zonally averaged meridional winds obtained by the MTGCM. Their adiabatic heating also reached much higher values: *Bougher et al.* [2006] reported an adiabatic heating close to the pole between 800 and 3000 K/d. This higher heating could be due to the different dust amount: *Bougher et al.* [2006] used the dust opacity obtained during the third year of TES observations, more dusty than the first year used in our simulation (see paper 1). However, *Bell et al.* [2007], using the MTGCM, obtained an adiabatic heating of 1200 K/d for a dust distribution given the TES year 1 (and 1500 K/d for TES year 3), still about double than that obtained with our model. In spite of this difference in the intensity of the interhemispheric circulation and the adiabatic heating, both models predict similar temperatures and a similar magnitude for the TPW. A possible explanation can be found in the differences between the radiative cooling schemes used in both models: while the MTGCM uses, for the 15 μm cooling scheme, the actual atmospheric atomic oxygen concentration, we use a fixed value, as explained in paper 1. This induces a more efficient cooling of the upper mesosphere–lower thermosphere in the MTGCM, which would compensate for the more intense adiabatic heating.

2.3. Tidal Structure

[24] Atmospheric tides are oscillations with periods that are subharmonics of a solar day. They are forced by the absorption of solar radiation. In the upper atmosphere, different tidal sources/effects can be distinguished: tides can be generated in situ by CO_2 NIR solar heating (mainly in the mesosphere) and by UV heating (mainly in the thermosphere), or there can be upward propagating tides originated by the absorption of visible radiation by the ground or the absorption of short-wave radiation by the airborne dust [*Angelats i Coll et al.*, 2004]. The tidal oscillations in the atmospheric fields may be expressed, following *Forbes et al.* [2002], as a superposition of different modes (n, s):

$$\sum_n \sum_s A_{n,s}(z,\theta)\cos\left(n\Omega t + s\lambda - \phi_{n,s}(z,\theta)\right) \qquad (1)$$

where t is the time in sols, z is the altitude, θ is the latitude, λ is the geographical longitude, s is the zonal wave number (positive/negative if the wave propagates westward/eastward), Ω is the planetary rotation rate, $A_{n,s}$ is the amplitude of the (n, s) mode (that is, half the magnitude of the peak-to-peak oscillation), $\phi_{n,s}$ is its phase, and n = 1 for the diurnal tide, n = 2 for the semidiurnal tide, and so on. Components with $n = s$ move with the apparent motion of the Sun and are called migrating components, while if $n \neq s$ then they are nonmigrating components. The migrating components are directly excited by a longitudinally invariant solar illumination, while the nonmigrating components can be forced via longitudinal variations in the solar heating associated with variations in surface thermal inertia, albedo and aerosols distributions, interactions of the migrating tide with topography [*Zurek*, 1976; *Wilson and Hamilton*, 1996], and as a result of nonlinear interactions with other waves [*Forbes*, 2002].

[25] We have performed a Fourier decomposition of the density structure predicted by our model to identify the most prominent waves present in the results of this simulation. This allows us to obtain the amplitude $A_{n,s}$ and the phase $\phi_{n,s}$ of each (n,s) component, as given by equation (1). Similar studies were made previously with GCMs [*Wilson*, 2002; *Angelats i Coll et al.*, 2004], but the upper limit of these models was set at about 120 km or below and did not allow for the study of the propagation of waves into the

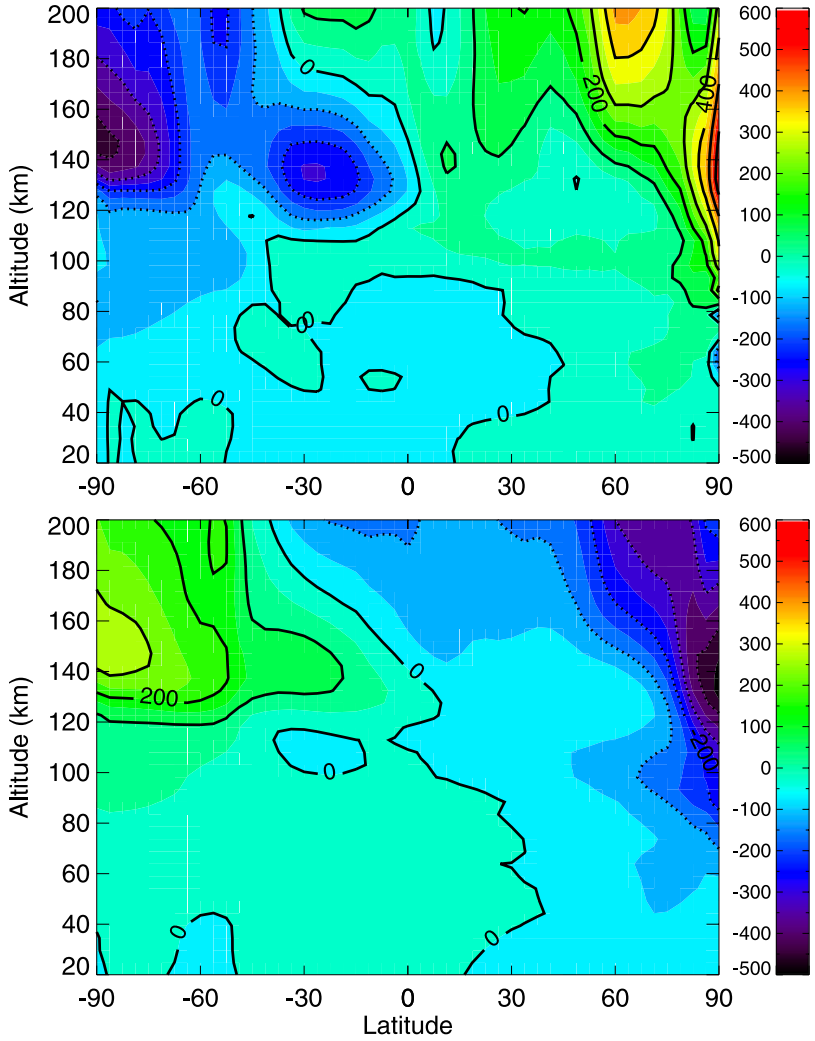

Figure 10. (top) Zonally averaged adiabatic heating predicted by the LMD-MGCM. (bottom) Sum of the zonally averaged heating terms presented in Figure 5. All in K/d, L_s = 270–300.

thermosphere, where they should have profound effects. *Bougher et al.* [1993] studied the effect of the propagating semidiurnal tide into the thermosphere although the generation of the tides was not self-consistently treated. It was instead included as a lower-boundary condition. *Forbes et al.* [2002] (hereafter, F2002) studied the propagation into the thermosphere of waves created in the lower atmosphere by the NASA/Ames GCM by using a mechanistic model, for which external temperature and wind fields had to be constructed by merging results from the NASA/Ames GCM and the MTGCM. This mechanistic model did not include the excitation of in situ tides at thermospheric altitudes (that is, they ignored those tides which are directly excited in the upper atmosphere). Two recent studies [*Moudden and Forbes*, 2008a, 2008b] have used the Global Mars Multiscale Model (GMMM), a general circulation model extending from the surface to about 160 km, to study the propagation of waves created in the lower atmosphere up to the thermosphere, and their effects on the circulation and thermal structure at thermospheric altitudes, for the L_s = 60 season. They find that eastward nonmigrating tides propagate easily up to the upper atmosphere, while their westward counterparts, with a shorter wavelength, tend to dissipate before reaching high altitudes.

[26] The density amplitudes for those components with higher amplitudes are depicted in Figure 11. They are normalized to the zonal mean density, so that if a mode has an amplitude of 0.2, it produces variations in density of ±20% of the zonal mean density. We use the notation (n, s) to identify each mode, so (1, 1) is the diurnal westward wave number 1 component, (2, −2) is the semidiurnal eastward wave number 2 component, and so on. The diurnal migrating tide (that is, the (1, 1) component), directly excited by the solar illumination, dominates in the upper thermosphere and at low latitudes, with a strong peak at about 120 km and another one above 200 km in the low and midlatitudes of the southern hemisphere. These two maxima are about 20 km higher than the maxima of the two main heating sources in the upper atmosphere, the UV heating and the NIR heating (Figure 5). This is expected, as the density structure at a given altitude reflects the integrated effect of the temperature in the lower layers. This component also has a significant amplitude in the winter pole. The other directly excited component, the migrating semidiurnal tide (2, 2), presents the same altitude structure of the

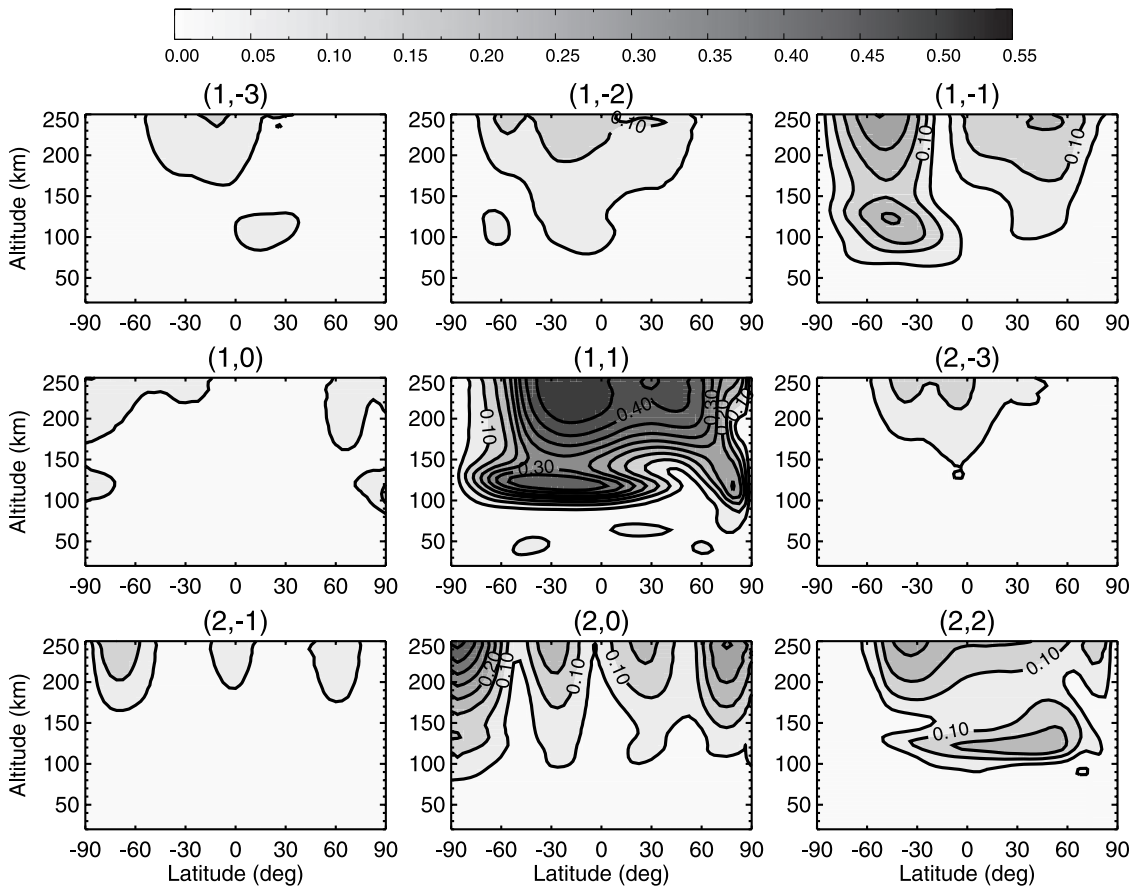

Figure 11. Relative density amplitude (normalized by the zonal mean values) at L_s = 270–300.

migrating diurnal tide, but has a lower amplitude, with a maximum of about 15% in mid-high latitudes in the winter hemisphere and another one in the upper layers of the summer hemisphere.

[27] Nonmigrating tides have an important contribution. In particular, the (1, −1) component has an amplitude of about 20% in the midlatitudes of the summer hemisphere. As commented in section 1, previous works have found that this component is a key factor in the creation of the wave-2 structure seen by MGS [*Forbes and Hagan*, 2000 (hereafter, FH2000); *Wilson*, 2002; *Angelats i Coll et al.*, 2004]. FH2000 find a higher amplitude for this component, of up to about 50%, for the same season. This component has also been studied for the L_s = 60 season by *Wilson* [2002] and *Moudden and Forbes* [2008b]. Both report significant amplitudes in the upper atmosphere. This component is created mainly by the interaction of the directly forced migrating tide with the topography, as shown by *Moudden and Forbes* [2008b]. Other nonmigrating components with significant amplitudes include (1, −3), (1, −2), (2, −3) (all with maximum amplitudes of about 10%), and especially (2, 0). The (1, −2) component is reported to have an 0.15 relative amplitude at 125 km for the L_s = 270 case in F2002, higher than predicted by our model. *Wilson* [2002] and *Moudden and Forbes* [2008b] also study this component for L_s = 60, reporting a maximum amplitude of about 0.25 in the equatorial region. The (2, 0) component has strong peaks in both polar regions, with higher amplitude (more than 30%) in the summer pole. This behavior is very similar to that presented in F2002 for this component for L_s = 30 and by *Moudden and Forbes* [2008b] for L_s = 60. However, F2002 reported a much weaker contribution of this component for L_s = 270.

[28] An important difference between the simulations in FH2000 and F2002 with that presented here is the structure of the zonally averaged zonal winds, shown in the Figure 7 (top), to be compared with Figure 1b of FH2000 and Figure 4 of F2002. As described in section 2.2, in the low-midmesosphere our model predicts strong eastward winds in the winter hemisphere (up to 100 m/s) that are progressively decelerated in upper layers, becoming very weak eastward or even westward winds in the upper thermosphere. In the summer hemisphere, intense westward winds are dominant at all altitudes, with maximum intensity of about 200 m/s in the middle atmosphere and about 150 m/s in the upper layers. In contrast, in FH2000 and F2002 the eastward jet in the summer hemisphere extends all over the thermosphere, and the intensity of the westward jet is about a factor of 2 lower than in our simulation. As the zonal wind structure has a strong influence on the propagation of tides [e.g., *Forbes*, 2002], these differences in the zonal winds could be at the origin of the differences in the wave structure.

[29] *Withers et al.* [2003] showed that the amplitude of the density tidal oscillations observed by MGS during its aerobraking decreases when going to altitudes of 130 to 160 km. Many of the components in Figure 11 show a peak at about 120 km and a minimum at about 160 km before

increasing again with altitude, in qualitative agreement with the observations.

3. Sensitivity Study: Role of Tides

3.1. In Situ Excited Migrating Tides

[30] As shown in section 2, our model reproduces the basic features of the observed TPW. This opens the door to further analysis that can shed some additional light on this phenomenon. We have performed a series of numerical experiments, changing some input parameters or some processes.

[31] First, a number of experiments modifying the dust opacity and/or its vertical distribution in our model produce results similar to those in the work by *Bell et al.* [2007], highlighting the importance of the dust heating in the lower atmosphere.

[32] In addition, here we aim, in particular, to clarify the role of the tides, which as shown in section 2.3 are important in creating the predicted dynamical structure of the upper atmosphere and thus do play a role in the TPW. A previous work by *Angelats i Coll et al.* [2004], using the version extended up to 120 km of the LMD-MGCM, showed that the suppression of the in situ tides created by the CO_2 NIR heating produced a strong modification of the zonally averaged zonal winds for $L_s = 65$. We perform here a similar analysis with the extended GCM presented in paper 1.

[33] For this purpose, we have performed a simulation for the $L_s = 270–300$ "months" suppressing the creation of in situ tides, but allowing for the creation of tides in the lower atmosphere and its propagation up to the thermosphere. The in situ tides are created by the diurnally varying heating terms that act locally at these altitudes: the heating due to the absorption of NIR radiation by CO_2 and the heating due to the absorption of solar UV radiation mostly by CO_2 and atomic oxygen. As shown in Figure 5, the CO_2 NIR solar heating peaks at about 110 km, while the more intense UV heating has its maximum intensity at about 180 km. The suppression of the tides generated by these terms is accomplished by imposing a diurnally averaged heating. In this way, there is no diurnal cycle, but the total amount of energy injected by these terms per day is the same as in the reference simulation.

[34] The wave decomposition for this simulation is shown in Figure 12. There are important differences with respect to the reference simulation shown in Figure 11. The diurnal migrating component (1, 1) has almost disappeared. This indicates that the peaks obtained for this component in the reference simulation were due to the direct excitation by the in situ NIR and UV heating, and that this component propagates only weakly from the lower atmosphere. The structure of the semidiurnal migrating tide (2, 2) is strongly modified. When the in situ sources are eliminated, the two areas of maximum amplitude at 120 km in the winter middle latitudes and in the upper layers in the summer middle latitudes disappear, replaced by a strong maximum of about 40% at high winter latitudes. This maximum has to be produced by the propagation from the lower atmosphere and shows an enhanced propagation of this component through the eastward jet, reinforced with respect to the reference simulation, as will be shown later in this section.

[35] In most cases, the amplitude of the nonmigrating components is only slightly modified. The most notable difference is the decrease of the amplitude of the (2, 0) component, especially in the polar regions. *Angelats i Coll et al.* [2004] proposes two possibilities for the presence of this component in the upper atmosphere: the interaction of the diurnal migrating tide with some nonmigrating components or the modulation of the semidiurnal tidal forcing with the topography. The decrease of its amplitude when the in situ tides are suppressed suggests that the first mechanism could be important. However, the results of *Moudden and Forbes* [2008b] point to the interaction of the semidiurnal migrating component with the topography as the origin of this component.

[36] Although in general the wave activity is reduced with respect to the reference simulation, the fact of having nonnegligible wave activity in the upper atmosphere in the absence of in situ sources shows the importance of treating carefully the coupling between the lower and the upper atmosphere.

[37] The zonally averaged temperatures for this simulation, expressed as a function of latitude and altitude, are shown in Figure 13, together with the effect of the in situ tides over the temperatures, i.e., the difference of temperature between the reference simulation and the simulation without in situ tides. Comparing with the structure predicted in the reference simulation (Figure 1), we can see that the zonal mean temperature in the lower atmosphere does not show important changes, whereas the zonally averaged upper atmospheric temperature structure is strongly modified. In this new simulation the temperatures in the thermosphere monotonically decrease from the summer ($\approx$310 K) to the winter pole ($\approx$170 K). It is evident from Figure 13 (bottom) that the in situ tides induce a more efficient transport of heat from the summer to the winter hemisphere, with stronger effects on the polar thermosphere. Note that the effects of the tides are seen as low as 40 km in the winter polar regions.

[38] The inspection of the increase of temperature with respect to latitude = 30°N, shown in Figure 14, shows that there is still a warming of 10–20 K at the mesopause altitude. However, this is an artifact of using altitude as the vertical coordinate and the contraction of the atmosphere during the polar night. As already commented in section 2, because of this contraction the mesopause is located at a lower altitude in the polar winter than in the rest of the planet. As a consequence, at the typical altitude of the mesopause in the low and midlatitude regions we will find, in the polar winter region, the hotter lower thermosphere. When using pressure coordinates to make a plot similar to Figure 14 (not shown), this apparent polar warming disappears. This shows the utility of using pressure coordinates for the study of the upper atmosphere. In this case, pressure coordinates allow the separation of the "artificial" increase of temperature due to the contraction of the atmosphere and the "physical" increase of temperature due to an adiabatic warming. However, it is clear that altitude coordinates are still the best when comparing with spacecraft aerobraking data that are fundamentally in altitude.

[39] To better understand the reason of this modification of the thermal structure by the in situ tides, we plot in Figure 15 the zonally averaged zonal and meridional winds

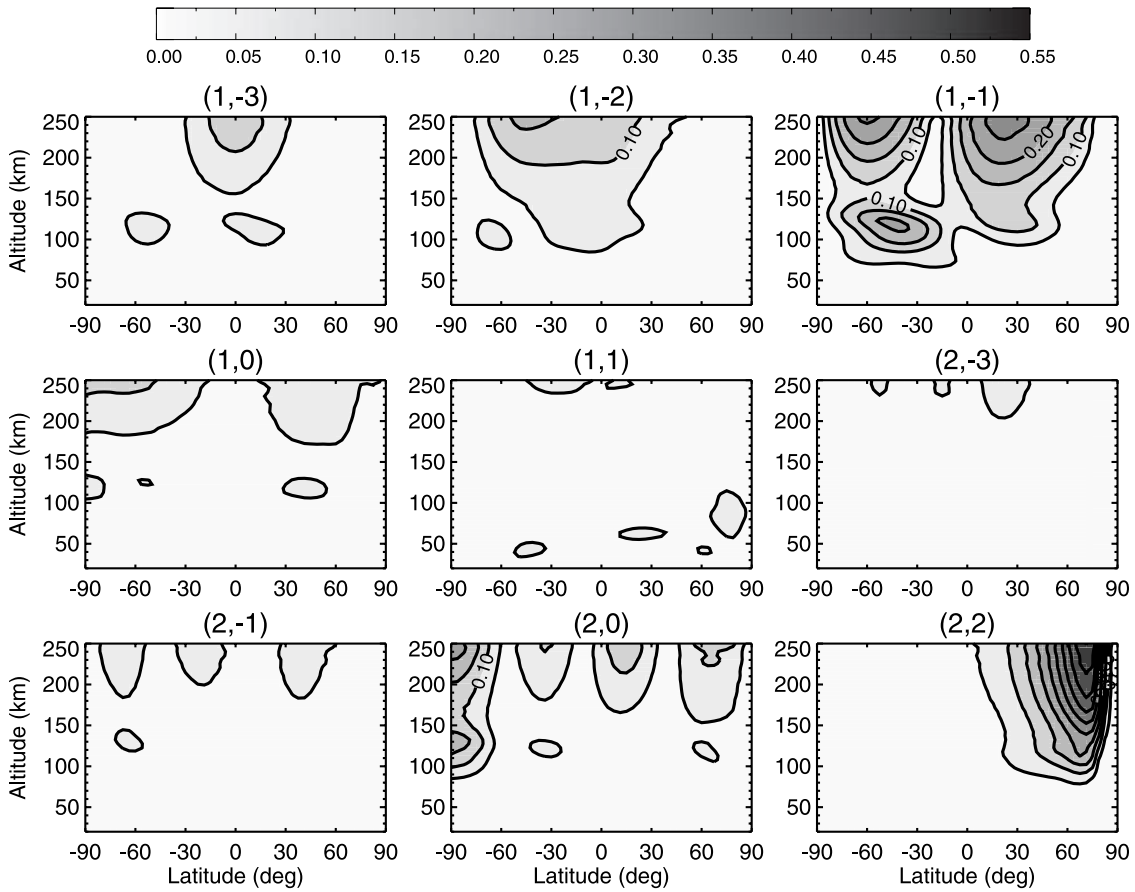

Figure 12. Relative density amplitude (normalized by the zonal mean values) at L_s = 270–300 with diurnally averaged in situ upper atmospheric heating.

at 120 km for this simulation as a function of local time and latitude. The intensity of the westward jet is strongly decreased with respect to the reference simulation (Figure 6), while the eastward winds in the winter polar region are reinforced. The meridional winds are radically modified: they are significantly decreased, and their structure completely modified. Weak northward winds are dominant at all regions, except in the northern hemisphere at the dayside. The divergence of winds in the dayside and convergence in the nightside that was dominant in the reference simulation has disappeared, and the interhemispheric transport is severely reduced. Maximum wind intensity is now about half that of the reference simulation. In the polar winter, a wave-2 structure is clearly seen in both the zonal and meridional wind.

[40] The reduction of the interhemispheric transport is confirmed by the analysis of the zonal mean winds. For the zonally averaged zonal wind, shown in Figure 16a, the main difference with respect to the reference simulation shown in Figure 7 is that the eastward jet in the winter hemisphere, that was previously confined to altitudes below about 120 km, now extends up to the thermosphere, even increasing its intensity with altitude reaching up to almost 200 m/s in the uppermost layers. When the in situ thermal tides are included, the zonally averaged zonal winds are more westward, especially in the winter pole (Figure 16b).

[41] The zonally averaged meridional winds are also modified: although the northward winds are still dominant at the mesopause level, their intensity is much lower than in the reference simulation, and there are areas dominated by southward winds. In particular, the meridional winds are much weaker in the polar region.

[42] What is producing this modification in the dynamical regime of the upper atmosphere? Let us have a look at the angular momentum in the upper atmosphere, shown in Figure 17 for the simulation without in situ tides, and in Figure 8 for the reference simulation, together with the mass stream function. A comparison of these two plots show clearly that the diurnal tides have an important contribution to the momentum budget: when the diurnal tides are included, the total angular momentum is lower, because of the deposition of the westward momentum carried by these waves. This modification of the angular momentum budget implies a modification of the horizontal winds. The zonal winds are modified and the meridional transport is strongly decreased with respect to the reference simulation. This is confirmed by the analysis of the mass stream function for both simulations. In the simulation with no tides, the stream function in the upper atmosphere winter pole is lower than in the reference simulation, which means that less mass is converging over the winter pole when the in situ tides are suppressed.

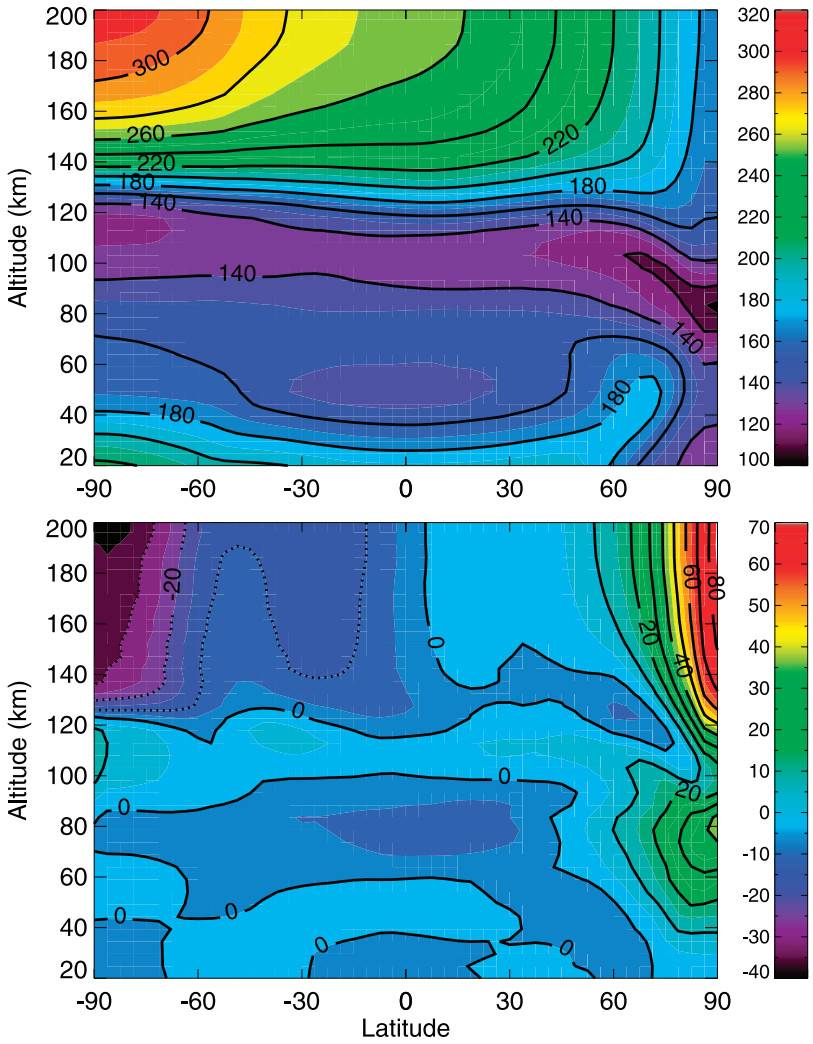

Figure 13. (top) Zonally averaged temperature (K) for a simulation using a diurnally averaged heating in the upper atmosphere. (bottom) Effect of in situ tides over the zonally averaged temperature (temperature of the reference simulation minus temperature of the simulation without in situ tides), in K. L_s = 270–300.

[43] The effects of tides on the circulation were already described in the work by *Wilson* [1997]. As mentioned above, *Angelats i Coll et al.* [2004] found a strong decrease of the westward winds when suppressing the creation of NIR tides at L_s = 65. *Forbes and Miyahara* [2006] found also that the semidiurnal migrating tide, created in the lower atmosphere during L_s = 270 and high dust opacity, deposited significant westward momentum in the thermosphere.

[44] The zonal mean vertical wind, shown in Figure 18 (top), is, as before, mainly upward in the summer hemisphere and downward in the winter one. However, the maximum downward wind in the polar mesopause, predicted in the reference simulation, is no longer present when the in situ tides are suppressed. In this case, the intensity of the downward wind is maximum in the upper thermosphere, but much smaller at the mesopause altitude. The depth of penetration from the thermosphere to the mesosphere is in consequence much lower than in the reference simulation.

[45] This, of course, has an effect on the adiabatic heating produced by this modified circulation. As shown in Figure 18 (bottom), now the adiabatic heating is confined to high altitudes, above about 160 km. At these altitudes, the molecular conduction is so efficient that this heating term has little effect over the temperatures. At 120–140 km, the adiabatic heating close to the winter pole is approximately 200–300 K/d, reduced to about one half with respect to the reference simulation. This reduced adiabatic heating is not strong enough to produce an appreciable TPW.

[46] We can thus conclude that the in situ tides created by the diurnally varying NIR and UV heating create a strong day-night temperature difference that imposes a strong dayside-nightside circulation, superimposed on the (solstitial) summer-to-winter circulation. This meridional circulation is characterized by a divergence of winds in the dayside low latitudes, with convergence in the nightside. These tides deposit their westward momentum in the thermosphere,

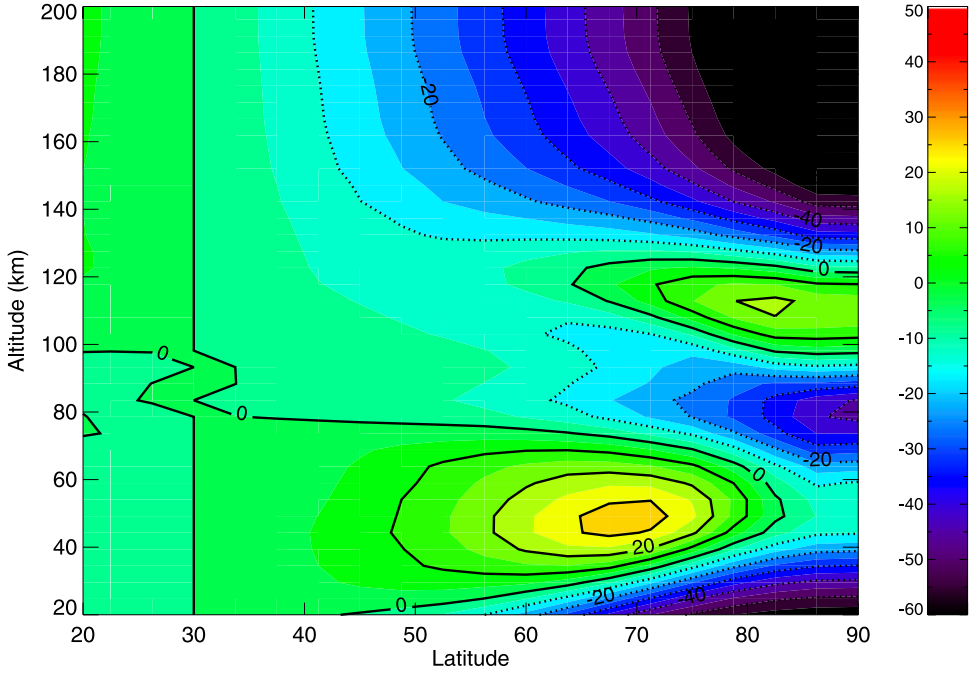

Figure 14. As in Figure 2, but for the simulation with suppressed in situ upper atmospheric tides.

modifying the momentum budget and as a consequence altering the horizontal winds. As a result, the meridional circulation is intensified, so that meridional winds can be as strong as 150 m/s, especially in the high latitudes. There is a convergence and descent of air over the polar night at the mesopause/lower thermosphere that produces a strong adiabatic warming that is at the origin of the TPW. There is a penetration of thermospheric air down to lower altitudes. When the in situ tides are suppressed, the dynamical structure is completely modified, the westward jet is weaker, and a strong eastward jet appears in the winter hemisphere. The zonal mean meridional wind is reduced, because of the wave-induced damping of the zonal mean flow. The interhemispheric transport and the convergence of air at the winter pole are radically diminished, as well as the penetration of air from the thermosphere to lower layers. The adiabatic heating at the polar night is strongly reduced, and no TPW is predicted.

[47] Further tests using a diurnal average for only one of the two heating terms in the upper atmosphere, the UV heating or the NIR heating (figure not shown), show that the tides originated by each of these heating terms produce a polar warming at slightly different altitudes (higher for the UV heating), but both of them complement each other to produce the observed TPW.

3.2. Upward Propagating Nonmigrating Tides

[48] As discussed in sections 1 and 2.3, the nonmigrating tides, that are excited in the lower atmosphere and can propagate up to thermospheric altitudes, have been shown to be important in the upper atmosphere. In particular, a recent study [*Moudden and Forbes*, 2008a] shows that these waves can have profound effects over the thermospheric dynamics. For the L_s = 60 season, they suggested that the westward winds are weakened and the eastward ones strengthened by the effects of nonmigrating waves propagating from the lower atmosphere. The meridional circulation and thus the thermal structure is also modified. It has to be remarked that, for this exercise, *Moudden and Forbes* [2008a] use a zonally averaged UV heating, which eliminates the migrating tides generated in situ at thermospheric altitudes.

[49] We make a similar exercise with our model for the L_s = 270–300 season. For this purpose, we use a flat, globally averaged topography, thermal inertia, and albedo, while keeping the diurnal solar cycle. In this way, the nonmigrating tides are not excited, but we keep the migrating tides excited both in the lower and the upper atmosphere. This will allow direct comparison with our reference simulation.

[50] The results of the simulation with globally averaged topography and surface properties are shown in Figure 19. The westward winds are stronger than in the reference simulation, in good qualitative agreement with the results shown by *Moudden and Forbes* [2008a], because of the absence of the nonmigrating tides. However, while *Moudden and Forbes* [2008a] find a strong impact in the zonal winds in the low-latitude region (up to 200 m/s at about 120 km), in our simulation the effect is more modest in the low latitudes, reaching significant intensity (up to about 120 m/s) in the polar winter. The meridional circulation is also modified by the elimination of the topography. Above about 140 km, areas with reinforced northward meridional wind alternate with areas of diminished wind. Between 60 and 120 km there is a clear effect of deceleration of the meridional wind by the elimination of the topography. These modifications in the dynamics have also an effect over the temperature structure. But while *Moudden and Forbes* [2008a] show a strong decrease of the polar temperatures above 100 km due to the nonmigrating tides,

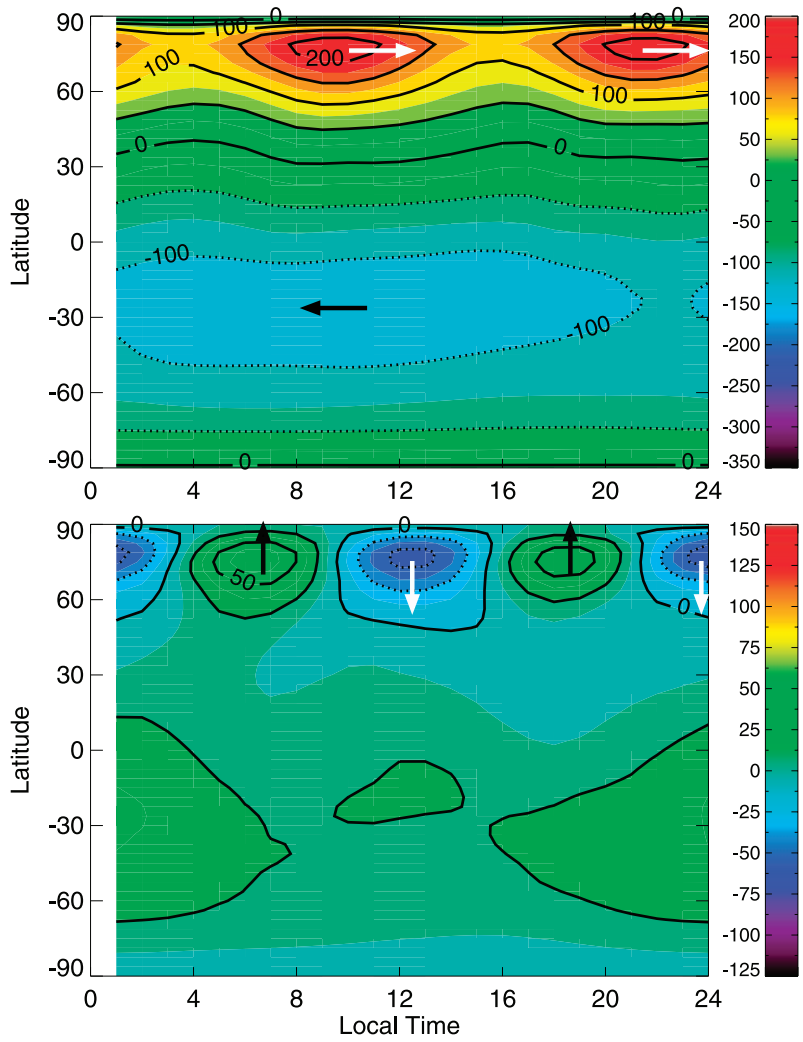

Figure 15. Longitude-latitude cross sections of the Sun-synchronous (top) zonal and (bottom) meridional winds (m/s) predicted by the model at 120 km for the simulation without in situ tides. Arrows have been added to show the wind direction. L_s = 270–300.

in our model the effect of the topography over the thermal structure is more modest, with differences of temperature with respect to the reference simulation limited to the polar winter region, and with a magnitude of about 20 K. These differences of temperature at the winter pole are positive above 100 km and negative below. In particular, it can be seen that the thermospheric polar warming is still present in this simulation (temperatures increase when going toward the winter pole below about 150 km), but its intensity and latitude-altitude distribution is modified with respect to the reference simulation.

[51] Can all these effects be attributed to the elimination of nonmigrating tides only, or do other factors have to be considered? As seen in Figure 19, the most important effects of eliminating the topography, both for the zonal winds and the temperature, are located close to the winter pole. However, Figure 11 shows that the density amplitude of the nonmigrating waves is small at these high latitudes. A similar wave decomposition for the zonal wind (figure not shown) shows also small magnitudes for the nonmigrating components close to the winter pole.

[52] In fact, using globally averaged topography and surface properties may affect other waves than nonmigrating tides. In particular, the transient and stationary waves will also be changed by this modification.

[53] A study of the day-to-day variability of the temperature for the reference simulation (Figure 20) shows an important transient wave activity for this season in the upper layers of the low and midlatitudes region of the summer hemisphere and in the polar region above about 60 km. A Hovmoller analysis (not shown) shows that this transient wave activity is dominated by a wave with a period of about 4 or 5 days that propagates to the west in the low and midlatitudes, while in the polar region the spectrum is dominated by a quasi-stationary wave with a period of about 7 days. A plot similar to Figure 20 for the simulation without topography (figure not shown) shows a similar behavior of the transient wave activity for the temperature at all latitudes except in the polar night, where the activity is

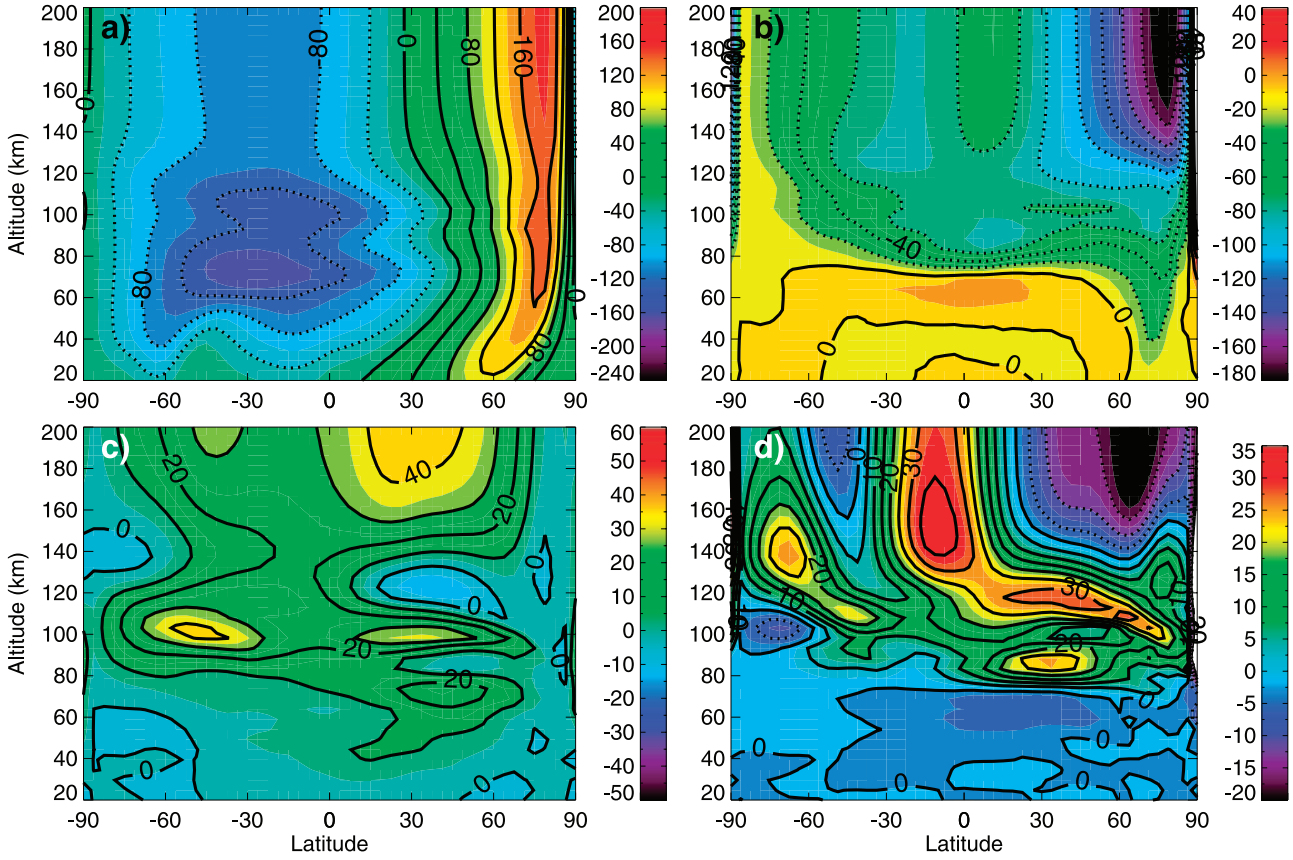

Figure 16. (a) Zonally averaged zonal wind for the simulation without in situ tides. (b) Effect of in situ tides over the zonally averaged zonal wind. (c) Zonally averaged meridional wind for the simulation without in situ tides. (d) Effect of the in situ tides over the zonally averaged meridional wind. All in m/s. L_s = 270–300.

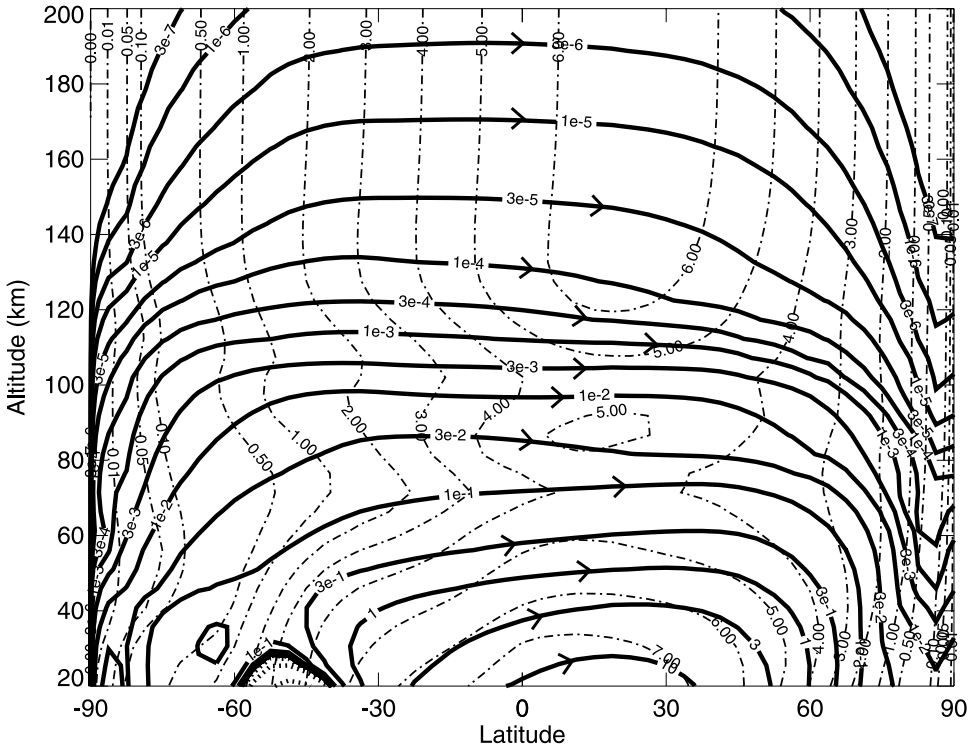

Figure 17. As in Figure 8, but for the simulation without in situ tides.

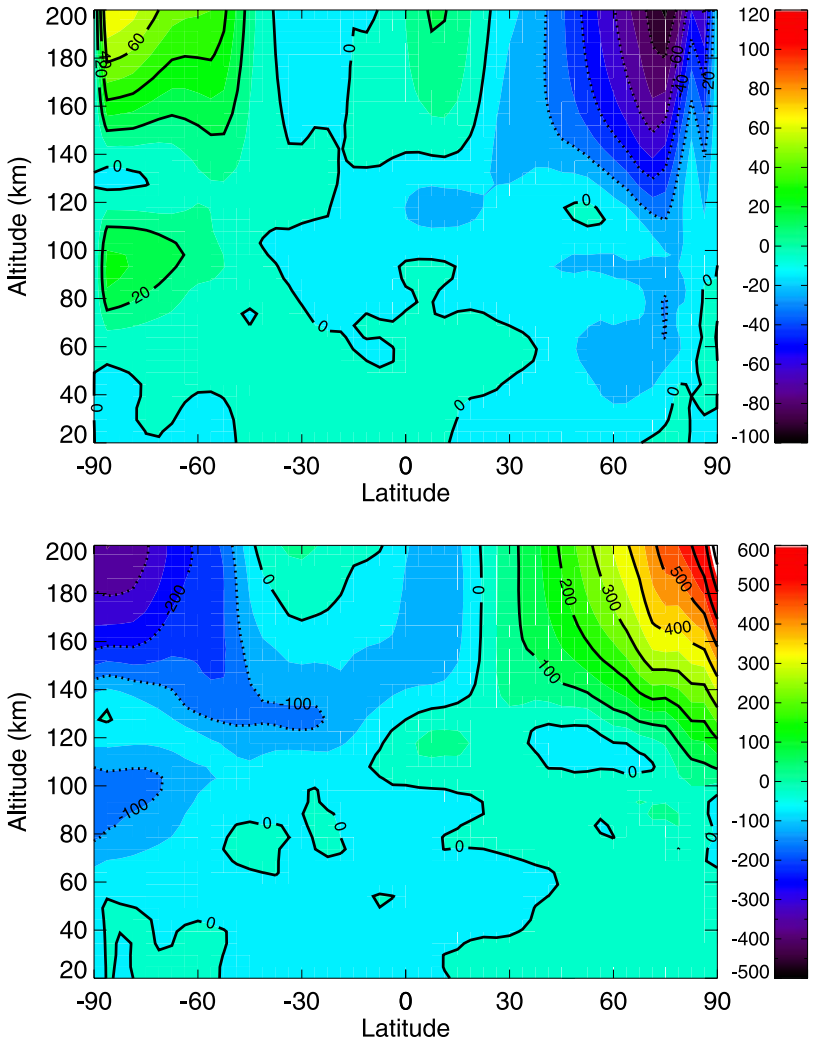

Figure 18. (top) Latitude-altitude cross section of the zonal mean vertical wind (cm/s, positive upward) for the simulation without in situ tides. (bottom) Latitude-altitude cross section of the zonally averaged adiabatic heating (K/d) for the simulation without in situ tides. L_s = 270–300.

strongly decreased. This indicates that at least part of the differences of temperature obtained when the topography is eliminated can be attributed to modifications in the transient wave activity, and not only to the effect of nonmigrating tides.

4. Summary and Perspectives

[54] The LMD-MGCM extended up to the thermosphere, described in paper 1, has been applied to the study of the temperature and wind structure in the upper atmosphere of Mars during southern summer solstice, focusing and those conditions consistent with the TPW first observed by Mars Odyssey.

[55] Predicted zonal mean temperatures at the mesopause/lower-thermosphere altitudes for the L_s = 270–300 seasons show evidences of a significant TPW. At 120 km, the temperatures increase by almost 50 K when going from latitude 30°N to the winter pole, a situation opposite to what would be expected by radiative equilibrium. This is in good agreement with the observations by Mars Odyssey, although the absolute value of temperatures are 30 K higher than observed.

[56] The analysis of the radiative heating terms and the thermal conduction confirms previous results that show that this TPW has a dynamic origin [*Bougher et al.*, 2006; *Bell et al.*, 2007]: there is a strong interhemispheric circulation from the summer to the winter hemisphere, enhanced by the predominant westward zonal winds. This circulation produces a convergence of mass over the winter pole, a descending motion of air (that can penetrate down to altitudes as low as 50 km), and as a consequence a compressional adiabatic heating.

[57] We have performed a tidal Fourier decomposition of the density structure predicted by our model. The diurnal migrating component, directly excited by the in situ absorption of NIR and UV solar radiation, is dominant at almost all latitudes. Important contributions are obtained also from nonmigrating components, like the diurnal Kelvin wave and the semidiurnal (2, 0) wave.

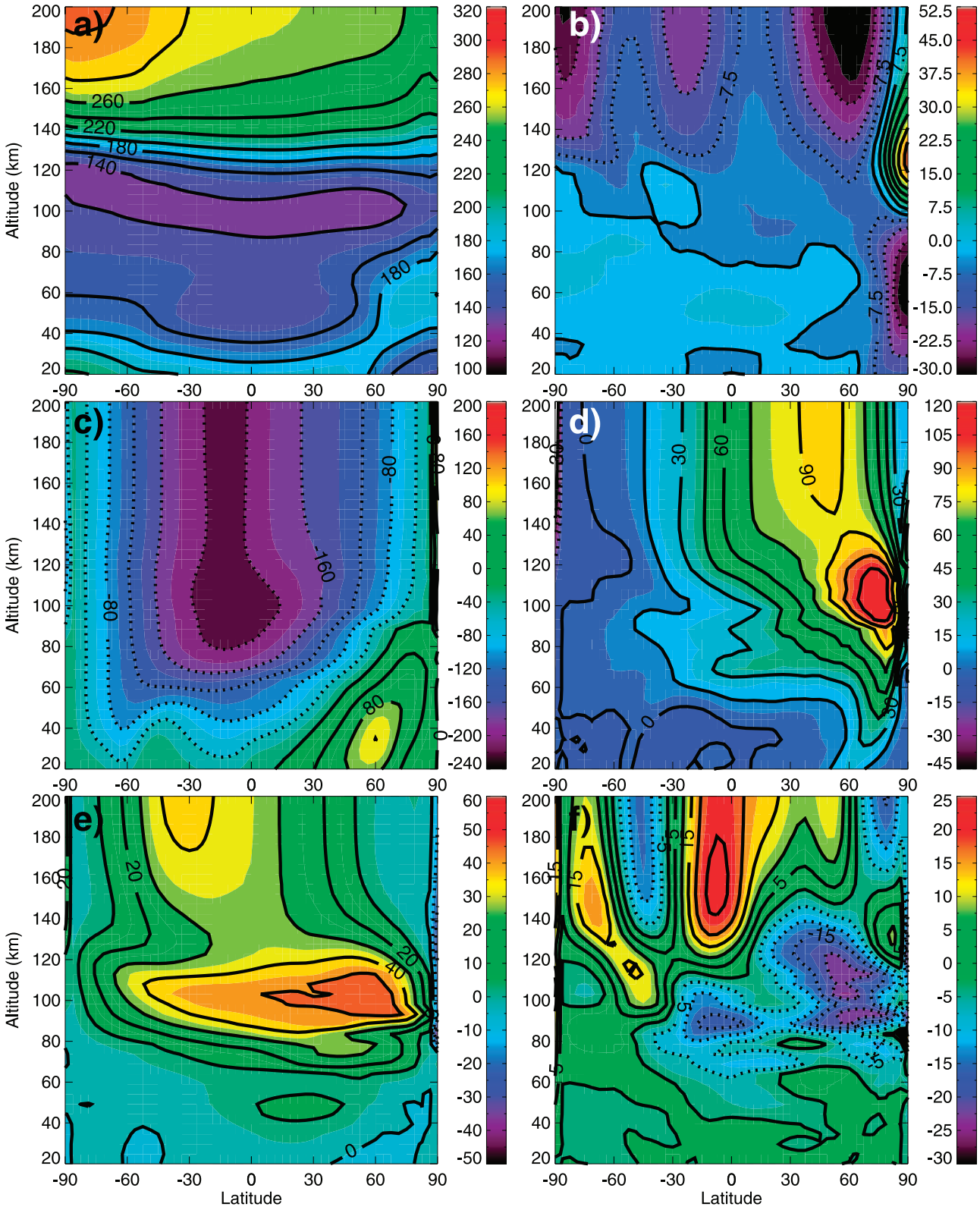

Figure 19. (a) Zonal mean temperature (K) for the simulation with globally averaged topography. (b) Effect of the topography over the zonal mean temperature ($T_{ref} - T_{notopo}$). (c) Zonally averaged zonal wind (m/s) for the simulation with globally averaged topography. (d) Effect of topography over the zonally averaged zonal wind ($u_{ref} - u_{notopo}$). (e) Zonally averaged meridional wind (m/s) for the simulation with globally averaged topography. (f) Effect of topography over the zonally averaged meridional wind ($v_{ref} - v_{notopo}$). L_s = 270–300.

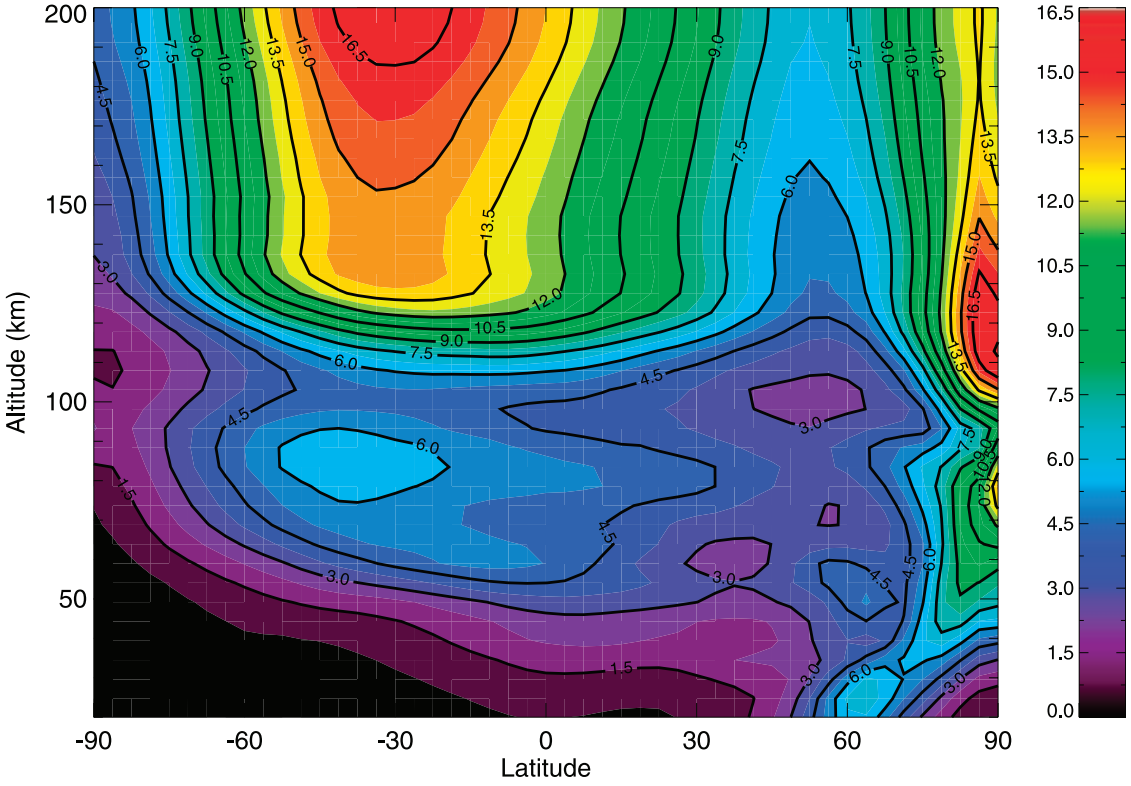

Figure 20. Zonal mean RMS of the temperature (K) for the reference simulation. L_s = 270–300.

[58] Regardless of the usual uncertainties in the IR balance due to the non-LTE nature of these molecular emissions, these terms are dominant in the upper mesosphere and the thermosphere, and they should have a strong influence over the simulated TPW. To check this, a simulation was made using a diurnally averaged NIR and UV heating, i.e., suppressing the creation of the in situ tides in the upper atmosphere. The tidal structure is modified: the in situ excited diurnal migrating tide is severely reduced, and the structure of the semidiurnal migrating tide is completely altered. The dynamical structure also exhibits a strong modification: a strong eastward wind jet appears in the upper atmosphere winter hemisphere, and the intensity of the meridional circulation, the convergence of air, and the descending motion over the pole are decreased, as well as the adiabatic heating. This produces the suppression of the TPW.

[59] The results of our simulations confirm the important role of the dynamics and the tides in determining the thermal structure of the upper atmosphere. In particular, we show the tides excited in situ by the absorption of NIR and UV solar radiation in the upper atmosphere are essential for the creation of the TPW.

[60] A simulation with globally averaged topography and surface properties shows also important modifications in the dynamical and thermal structure of the upper atmosphere, modifying in particular the intensity and altitude of the TPW. It is shown that this effect is not only due to the suppression of the nonmigrating upward propagating tides, but also to the modification of the transient wave activity.

[61] This study shows the capabilities of the ground-to-thermosphere LMD-MGCM to study, for the first time in a self-consistent way, the different couplings between physical processes and different altitude layers, that the latest observations have shown to be very important.

[62] **Acknowledgments.** The authors wish to thank John Wilson and an anonymous reviewer for their useful comments that contributed to significantly improve the paper. M.A.L.-V. was supported by Spanish Ministerio de Educacion y Ciencia under project AYA-2008-03498.

References

Angelats i Coll, M., F. Forget, M. A. López-Valverde, P. L. Read, and S. Lewis (2004), Upper atmosphere of Mars up to 120 km: Mars Global Surveyor data analysis with the LMD general circulation model, *J. Geophys. Res.*, *109*, E01011, doi:10.1029/2003JE002163.

Angelats i Coll, M., F. Forget, M. A. López-Valverde, and F. González-Galindo (2005), The first Mars thermospheric general circulation model: The Martian atmosphere from the ground to 240 km, *Geophys. Res. Lett.*, *32*, L04201, doi:10.1029/2004GL021368.

Bell, J. M., S. W. Bougher, and J. R. Murphy (2007), Vertical dust mixing and the interannual variations in the Mars thermosphere, *J. Geophys. Res.*, *112*, E12002, doi:10.1029/2006JE002856.

Bougher, S. W., C. G. Fesen, E. C. Ridley, and R. W. Zurek (1993), Mars mesosphere and thermosphere coupling: Semidiurnal tides, *J. Geophys. Res.*, *98*, 3281–3295.

Bougher, S. W., S. Engel, R. G. Roble, and B. Foster (1999), Comparative terrestrial planet thermosphere: 2. Solar cycle variation of global structure and winds at equinox, *J. Geophys. Res.*, *104*, 16,591–16,611.

Bougher, S. W., S. Engel, R. G. Roble, and B. Foster (2000), Comparative terrestrial planet thermospheres: 3. Solar cycle variation of global structure and winds at solstices, *J. Geophys. Res.*, *105*, 17,669–17,692.

Bougher, S. W., S. Engel, D. P. Hinson, and J. R. Murphy (2004), MGS Radio Science electron density profiles: Interannual variability and implications for the Martian neutral atmosphere, *J. Geophys. Res.*, *109*, E03010, doi:10.1029/2003JE002154.

Bougher, S. W., J. M. Bell, J. R. Murphy, M. A. López-Valverde, and P. G. Withers (2006), Polar warming in the Mars thermosphere: Seasonal variations owing to changing insolation and dust distributions, *Geophys. Res. Lett.*, *33*, L02203, doi:10.1029/2005GL024059.

Bougher, S. W., P.-L. Blelly, M. Combi, J. L. Fox, I. Mueller-Wodarg, A. Ridley, and R. G. Roble (2008), Neutral upper atmosphere and ionosphere modeling, *Space Sci. Rev.*, *139*, 107–141, doi:10.1007/s11214-008-9383-7.

Forbes, J. M. (2002), Wave coupling in terrestrial planetary atmospheres, in *Atmospheres in the Solar System: Comparative Aeronomy*, *Geophys. Monogr. Ser*, vol. 130, edited by M. Mendillo, A. Nagy, and J. H. Waite, pp. 171–190, AGU, Washington, D. C.

Forbes, J. M. (2004), Tides in the middle and upper atmospheres of Mars and Venus, *Adv. Space Res.*, *33*, 125–131.

Forbes, J. M., and M. E. Hagan (2000), Diurnal Kelvin wave in the atmosphere of Mars: Towards an understanding of "stationary" density structures observed by MGS accelerometer, *Geophys. Res. Lett.*, *27*, 3563–3566.

Forbes, J. M., and S. Miyahara (2006), Solar semidiurnal tide in the dusty atmosphere of Mars, *J. Atmos. Sci.*, *63*, 1798–1817.

Forbes, J. M., A. F. C. Bridger, S. W. Bougher, M. E. Hagan, J. L. Hollingsworth, G. M. Keating, and J. Murphy (2002), Nonmigrating tides in the thermosphere of Mars, *J. Geophys. Res.*, *107*(E11), 5113, doi:10.1029/2001JE001582.

Forget, F., F. Hourdin, R. Fournier, C. Hourdin, and O. Talagrand (1999), Improved general circulation models of the Martian atmosphere from the surface to above 80 km, *J. Geophys. Res.*, *104*, 24,155–24,175.

Forget, F., F. Montmessin, J. Bertaux, F. González-Galindo, S. Lebonnois, E. Quémerais, A. Reberac, E. Dimarellis, and M. A. López-Valverde (2009), The density and temperatures of the upper martian atmosphere measured by stellar occultations with Mars Express SPICAM, *J. Geophys. Res.*, *114*, E01004, doi:10.1029/2008JE003086.

González-Galindo, F., F. Forget, M. A. López-Valverde, M. Angelats i Coll, and E. Millour (2009), A ground-to-exosphere Martian general circulation model: 1. Seasonal, diurnal and solar cycle variation of thermospheric temperatures, *J. Geophys. Res.*, *114*, E04001, doi:10.1029/2008JE003246.

Jakoski, B. M., and T. Z. Martin (1987), Mars: North-polar atmospheric warming during dust storms, *Icarus*, *72*, 528–534.

Keating, G. M., M. Theriot, R. Tolson, S. W. Bougher, F. Forget, and J. Forbes (2003), Brief review of the results obtained with the MGS and Mars Odyssey 2001 accelerometer experiments, paper presented at the Mars Atmosphere: Modelling and Observations Workshop, Eur. Space Agency, Granada, Spain, 13–15 January.

Keating, G. M., S. W. Bougher, M. E. Theriot, R. H. Tolson, and J. M. Forbes (2008), Response of the Mars thermosphere to dynamical effects, AGU Fall Meeting Abstracts.

Lillis, R. J., S. W. Bougher, D. L. Mitchell, D. A. Brain, R. P. Lin, and M. H. Acua (2008), Continuous monitoring of nightside upper thermospheric mass densities in the Martian southern hemisphere over 4 Martian years using electron reflectometry, *Icarus*, *194*, 562–574, doi:10.1016/j.icarus.2007.09.031.

López-Puertas, M., and M. A. López-Valverde (1995), Radiative energy balance of CO_2 Non-LTE infrared emissions in the Martian atmosphere, *Icarus*, *114*, 113–129.

Moudden, Y., and J. M. Forbes (2008a), Effects of vertically propagating thermal tides on the mean structure and dynamics of Mars's lower thermosphere, *Geophys. Res. Lett.*, *35*, L23805, doi:10.1029/2008GL036086.

Moudden, Y., and J. M. Forbes (2008b), Topographic connections with density waves in Mars' aerobraking regime, *J. Geophys. Res.*, *113*, E11009, doi:10.1029/2008JE003107.

Smith, M. D., J. C. Pearl, B. J. Conrath, and P. R. Christensen (2001), Thermal Emission Spectrometer results: Mars atmospheric thermal structure and aerosol distribution, *J. Geophys. Res.*, *106*, 23,929–23,945.

Wilson, R. J. (1997), A general circulation model simulation of the Martian polar warming, *Geophys. Res. Lett.*, *24*, 123–127.

Wilson, R. J. (2000), Evidence for diurnal period Kelvin waves in the Martian atmosphere from Mars Global Surveyor TES data, *Geophys. Res. Lett.*, *27*, 3889–3892.

Wilson, R. J. (2002), Evidence for nonmigrating thermal tides in the Mars upper atmosphere from the Mars Global Surveyor Accelerometer Experiment, *Geophys. Res. Lett.*, *29*(7), 1120, doi:10.1029/2001GL013975.

Wilson, R. J., and K. Hamilton (1996), Comprehensive model simulation of thermal tides in the Martian atmosphere, *J. Atmos. Sci.*, *53*, 1290–1326.

Withers, P., S. W. Bougher, and G. M. Keating (2003), The effects of topographically-controlled thermal tides in the Martian upper atmosphere as seen by the MGS accelerometer, *Icarus*, *164*, 14–32.

Zurek, R. W. (1976), Diurnal tide in the martian atmosphere, *J. Atmos. Sci.*, *33*, 321–327.

M. Angelats i Coll, F. Forget, and F. González-Galindo, Laboratoire de Météorologie Dynamique, Institute Pierre Simon Laplace, 4 Place Jussieu, Paris F-85721, France. (fgglmd@lmd.jussieu.fr)

M. A. López-Valverde, Instituto de Astrofísica de Andalucía, CSIC, Camino Bajo de Huétor 50, E-18008 Granada, Spain.